both Japan and Japanese living abroad would become terrorist targets.7 In response to the mailborne anthrax terrorist attacks in the United States, the Ministry of Health, Labor and Welfare of the Japanese government has formed a working group on protection against bioterrorism in December 2001, and has started preparing mass production of vaccine against smallpox for 10 million civilian persons using less neuropathogenic tissue culture freeze-dried vaccine with LC16m8 strain.9 The Ministry has also begun to prepare vaccines for first-line health care workers in case of smallpox bioterrorism. The Self Defense Force personnel who are serving in peace-keeping operations in the Middle Eastern countries have already been vaccinated. Although the Ministry has announced a contingency plan for a possible outbreak of smallpox in Japan,10 detailed information and guidelines are still lacking when compared to the ones produced by the CDC. Although the Japanese government prepared its plan using much from the CDC, unlike CDC, it has neither given the scientific justification in their policy for amount of the vaccines necessary, nor provided the reason why post-exposure vaccination should be carried out within the four days after exposure. Because the Japanese government has not made it clear to the public its policy and intention regarding the smallpox vaccination, the public until date remains ignorant and thus unprepared.

In the face of many unknowns, several mathematical epidemiologists have challenged the presently used models for assessing public health interventions including the vaccination policy regarding the survival and spread of smallpox, "LIZLIAM or for estimating its transmissibility using past epidemiologic records. 15.16 Models may be conceptualized as thought experiments, and are extremely useful tools when physical experiments are impossible

to perform due to time, monetary, practical, or ethical constraints." The purposes of this study are to simulate the possible scenarios which could arise from a bioterrorist attack of introducing smallpox into Japan, and to describe the possible outcome of different nationwide vaccination policies based on the hypothesis on residual immunity in the population. This would allow the Japanese government to impose its original vaccination policy, and determine what new epidemiologic study is needed.

#### **METHODS**

### Mathematical Model

The analysis presented in this paper is based on a deterministic mathematical model for epidemic which could predict the epidemiologic outcome while simultaneously evaluating the effect of any specified control strategy on smallpox. The model is a modification of the SEIJR model,18 which separates the population into the classes of people who are susceptible (S), exposed (E), infectious (I), diagnosed (J), and recovered (R). The model is described by a set of ordinal differential equations which are based upon specific biological and intervention assumptions about the transmission dynamics of smallpox (Figure 1). We first separate the susceptible population (S) into three age groups according to the expected immunity:19 (Group A) represents those who have never been vaccinated (Sa) i.e., born after 1977, and who constitute the proportion (1-x-y) of the total population, (Group B) represents those who received only primary vaccination (SB) i.e., born between 1969-1977, and is denoted as xN, and (Group C) represents those who have received both primary and revaccination (Sc) i.e., born before 1969, and is denoted as yN. A

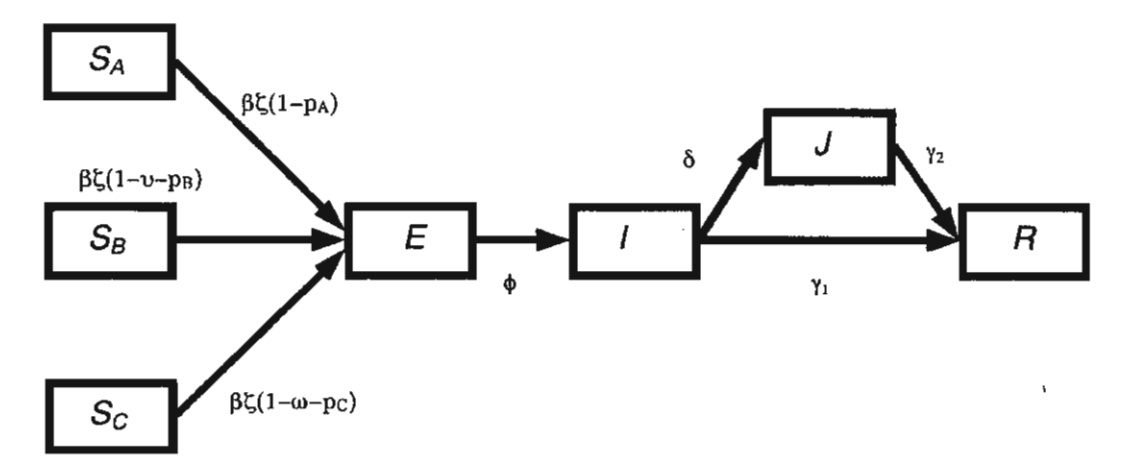


Figure 1. The transmission dynamics of the smallpox taking into account the impact of different residual immunity and interventions.

Here: SA, SB and SC represents the proportion of population susceptible among Groups A (born after 1977), B (born in 1969-1977), and C (born before 1969), respectively; E represents the proportion of untraced latent individuals; I the proportion of the population infectious; J the proportion of infectious isolated; R the proportion of recovered and death.

certain proportion from each population groups (A, B, and C) are assumed to be effectively protected by present vaccination strategy, and denoted as ps. ps , and pc. A smallpox infection among the susceptible population (SA, SB, and Sc) firstly begins with a non-infectious incubation period (E), which constitute the latency period. It would be followed by prodrome with non-specific symptoms, and by an overtly infectious (I) and symptomatic stage, characterized by a pustular rash. By this time, most of infections would be apparent and be diagnosed (J). The patients would then either slowly recover or die (R).20 While infectious, the infected patients can transmit the disease to other susceptible individuals at a rate dependent on the basic reproduction number, Ro.21 There are currently three possible public health interventions for interrupting the transmission of the virus. These are (1) vaccinating those who are at risk or may have already been exposed, (2) quarantining certain proportion of those who are known to have been exposed and therefore may be infected but are not yet ill (see Appendix), and (3) moving infectious individuals (1) into isolation after being diagnosed (J). We assume that each susceptible makes  $\zeta$  contacts per day with an infectious person. Among the known contacts (in SA, SB, and Sc), some would be infected with the probability of  $\beta$  per contacts (and enter into E) and  $(I - \beta)$ remains uninfected and susceptible. Untraced infectious persons would recover or die after ( y 1)" days. Apparent infectious person would be diagnosed and isolated with the mean daily rate  $\delta$ (and enter into J), and recover or die  $(y_2)^{-1}$  days after isolation. Because isolation can never be perfect, we estimate that those who are isolated also contribute to the generation of newly infected cases. Therefore, relative measure of reduced risk among those isolated ( $\pi$ ) is multiplied to J. These processes can be modeled using an approximately parameterized set of differential equations [1] as given by:

$$\frac{dS_A}{dt} = -\zeta \beta (1 - p_A) S_A (I + \pi J)$$

$$\frac{dS_B}{dt} = -\zeta \beta (1 - \nu - p_B) S_B (I + \pi J)$$

$$\frac{dS_C}{dt} = -\zeta \beta (1 - \omega - p_C) S_C (I + \pi J)$$

$$\frac{dE}{dt} = -\beta \zeta \left\{ (1 - p_A) S_A + (1 - \nu - p_B) S_B + (1 - \omega - p_C) S_C \right\} (I + \pi J) - \phi E \quad [1]$$

$$\frac{dI}{dt} = \phi E - (\gamma_1 + \delta) I$$

$$\frac{dJ}{dt} = \delta I - \gamma_2 J$$

$$\frac{dR}{dt} = \gamma_1 I + \gamma_2 J$$

Because isolation measure is not usually undertaken in the early stage of the epidemic (the stage of which is given by  $S_A + S_B + S_C = N$  and (E(t), I(t), J(t)) = (0, 0, 0), where N is the size of the population in which the epidemic occurs), I(t) at the initial attack with-

out the effect of quarantine would be given by:

$$\frac{dE(t)}{dt} = \left[\beta\zeta\left\{(1-p_A)S_A(0) + (1-v-p_B)S_B(0) + (1-\omega-p_C)S_C(0)\right\} - \gamma_1\right]I(t) \quad [2]$$

Therefore, the growth of infectious person at initial stage will follow Malthusian model as follows:

$$I(t) = I(0)e^{\int \beta \zeta \{(1-\rho_A)S_A(0) + (1-\nu-\rho_B)S_B(0) + (1-\omega-\rho_C)S_C(0)\} - \gamma_1\}}$$
[3]

From the second generator approach,<sup>22</sup> we obtain the following expression for the basic reproduction number, Ro:

$$R_{0} = \zeta \beta N \left\{ (1 - p_{A}) (1 - x - y) + (1 - v - p_{B})x + (I - \omega - p_{C})y \right\} \times \left\{ \frac{1}{\delta + \gamma_{1}} + \frac{\delta \pi}{\gamma_{2}(\delta + \gamma_{1})} \right\}$$
[4]

A description of the other principal parameters in the model and of their assigned value is presented below.

#### Parameter Values

Table 1 contains the parameter values for our baseline case. Assuming that the biological variables do not differ much from those of past epidemics, we use the values given in previous epidemic modeling studies 12,13,15,66 for possible scenario analyses. The infection rate  $\beta \zeta$  is chosen and fixed so that  $R_0 = 6.87$ , which is derived from an estimate on the order of 4.52 to 10.1 estimated in the previous study that have involved calculation of Ro." Because our purposes here are to draw crude pictures of the possible smallpox bioterrorist attack and describe the impact of residual immunity, we performed an analysis based on a single value of Ro (although we have varied parameter assumption in sensitivity analysis for assumed residual immunity and initial attack size discussed below). These types of analyses on the impact of public health interventions are beyond the scope of this paper. Such studies have already been undertaken elsewhere. "" Therefore, our simulation itself in this paper excludes the effect of quarantine (see Appendix, where we formulated the model incorporating the effect of quarantine). We assume that the pattern of contact is linearly related to the population size so that every infectious person will pass the disease to exactly Ro susceptible individuals simultaneously within an incubation period of  $(\phi)^{-1}$  days. From this assumption,  $\zeta N$  denotes the daily number of contacts in the population. In addition, we use a single value of Ro throughout the epidemic that represents the post-detection scenario so as to estimate the natural course (without interventions) of the epidemic although the transmission rate is likely to decrease after the epidemic is detected and announced. Although homogenous (or free) mixing is not an accurate description of the actual population interactions, free mixing usually leads to larger epidemics than nonrandom mixing.23 In addition, we assumed homogenous mixing because smallpox infections as caused by a bioterrorist attack would not necessarily accumulate in a small number of limited locations. We start the bioterrorism scenario with an entry of 10 initial cases into a population of 1,000,000 people, with enough population density to give the more than necessary critical proportion of the population, as our baseline case. It is assumed that one million people with a certain population density is a typical representation of a population of one ward in an urban area in Japan (i.e., Setagaya ward of Tokyo has a population of 815,000). It is somewhat unrealistic to expect the population at the prefectural or national level to be at risk because it would not be possible to have 100% of this population to come into possible direct or indirect contact with the disease within the short time period of

concern. We have therefore considered a scenario of an epidemic in a city or ward sized population, such as the one of Setagaya.

We first simulate three possible scenarios for different proportion of people whose residual immunity still exist. In the first scenario, based on the hypothetical long-lasting immunity in Japan's estimated using latest study in India, we assume that approximately 30% of Group B and 90% of Group C (with population size of  $1.05 \times 10^6$  and  $6.01 \times 10^6$ , respectively) will still have protective immunity against smallpox. The proportion of people with immunity in Group B (v) and C ( $\omega$ ) would thus be set as 0.30

Table 1. Parameter values for transmission dynamics of smallpox.

Parameters	Description	Baseline Values	Referrence	
β	The probability of transmission per contacts	$\beta \zeta = 4.26$		
ζ	The daily number of contacts per capita		*a	
рл	The proportion of exposed person among Group A who was effectively protected by vaccination	0.00	*b	
ps	The proportion of exposed person among Group B who was effectively protected by vaccination	0.00	*b	
рc	The proportion of exposed person among Group C who was effectively protected by vaccination	0.00	*b	
φ	The average rate at which latent individuals become infectious	0.0685 day <sup>.1</sup>	3	
δ	The mean daily rate at which infectious cases are diagnosed and isolated	0.95 day <sup>-1</sup>	3	
γι	The percapita rate for recovery and deth	0.116 day-1	27	
у2	The percapita rate for recovery and deth after isolated	0.132 day-1	3,28	
π	Relative measure of reduced risk among isolated cases	0.10	16,29	
x	The proportion of Group B population	0.105	19	
y	The proportion of Group C population	0.601	19	
υ	The proportion of population with residual immunity among Group B estimated	0.30	19,24	
ω	The proportion of population with residual immunity among Group C estimated	0.90	19	

<sup>\*</sup>a: The infection rate  $\beta \zeta$  is chosen and fixed so that the basic reproduction number becomes 6.87.

<sup>\*</sup>b: Projected epidemic curves (baseline case) given by simulation ignored vaccination.

Discussion for these parameters are given in text.

and 0.90, respectively. Because Group A consists of only those who were born in 1977 and thereafter have never been vaccinated, no one in this group will have the protective immunity. For the second scenario, we assume that half of estimated population still possesses immunity (v = 0.15, w = 0.45). It is believed that loss of immune protection might contribute to the epidemic. For the third scenario, we assume that no person possess protective immunity (v = 0, w = 0). To make the differences between those three scenarios clearly visible, we assume that there is no public health intervention except isolation in all three scenarios.

"We then consider the impact of different levels of vaccine distributions for the three age groups (A, B, and C), which would become crucial if nationwide mass-vaccination is required (level III). By estimating the optimal condition in order to prioritize, we generalize the condition with simple mathematical formula so that it can be applied to other communities having different age distribution. Finally, we estimate the total amount of smallpox vaccines needed in Japan using a generalized formula. In this study, the total number of people in the population is assumed to be constant during the epidemic. The background mortality rate is assumed to be negligible over the time periods examined.

#### Sensitivity analysis

Because model parameters regarding the proportion of the population in Groups B and C with residual immunity (v,  $\omega$ ) and initial attack size (1(0)N) possess the most uncertainty, a sensitivity analysis comparing the reproduction number is performed for different settings of them. Firstly, we compare the sensitivity of the reproduction number for either v or  $\omega$ , and then varied both. In three of the comparisons, both v and  $\omega$  are varied from 0 to 1.0 separately. When we vary both of them, we multiplied the relative reliability, which we define as a variable from 0 to 1.0, to our assumed immune proportion ( v = 0.30 or  $\omega = 0.90$ ). As for the initial attack size, we analyzed the reproduction number by varying I(0)N from 10 to 100,000 cases. A hundred thousand is selected as the maximum number of initial cases because it would be 10% of the total population. Whatever the way of introduction would be, we consider it is unrealistic to assume much more number of initial cases in our assumed ward-sized community.

### **RESULTS**

The result of a simple scenario analysis is seen in Figure 2. It shows the probable dynamics of the smallpox epidemics under different conditions of residual immunity. The results are given for up to 50 days after the onset of epidemic. It is unrealistic to estimate for longer period of time because one would not expect the health policy and control strategies as well as social reactions to remain static over longer periods. Without any public health interventions and protective immunity, exponential growth of daily number of new cases would occur. The point prevalence (here denoted as the number of infectious individuals) would exceed 500 persons by the 33rd day after onset of epidemic. If the

half of estimated immune population in Groups B and C still possesses immunity, the incidence rate (=rapidity) of smallpox will be lessened, but the trend of exponential growth would not cease without any interventions. On the other hand, the daily number of new cases would be in relatively controllable number if parts of the Groups B and C were perfectly immune as hypothesized. It is notable that trend of increase would still be observed without interventions. The difference in the prevalence between a population which had no immunity and the one which had the expected immunity at 50th day would be approximately 405 folds.

If a proportion p of the population is successfully immunized, the critical proportion of the population to be immunized ( $p_{cri}$ ), which is needed to attain the eradication,<sup>21</sup> is given simply by:

$$p_{cri} = 1 - \frac{1}{R_0}$$
 [5]

Approximate estimate of the vaccination coverage (the degree of herd immunity) needed to eradicate smallpox is known to be in the order of 70 to 80%. Here, we separate the susceptible into three age groups based on their possible residual immunity. Based on this assumption, the condition to break the chain in the person-

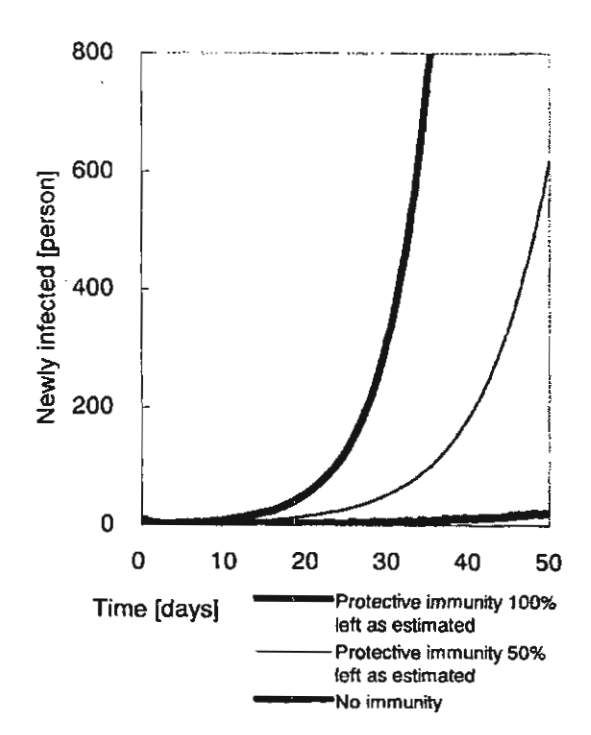


Figure 2. Dynamics of a smallpox attack with the basic reproduction number Ra = 6.87.

The number of infectious smallpox cases according to the protective (residual) immunity in Groups B (born in 1969-1977) and C (born before 1969), v and  $\omega$ . Simulations were performed with a time-step of 0.1 days.

to-person transmission of smallpox is given by the equation [4]:

$$(1-p_A) \left(1-x-y\right) + (1-v-p_B) x + (1-\omega-pc) y < \frac{1}{R_0} \qquad [6]$$

where x and y are the proportion of Groups B and C in susceptible population, respectively. Population of the Group A can be represented as (1-x-y)N. If the hypothesized level of immunity were perfectly realistic (such as our baseline case, v = 0.30 and w = 0.90 described in Table 1), the prioritization in order to achieve the most effective vaccine intervention can be calculated by:

$$f(p) = (1 - x - y) p_A + xp_B + yp_C$$
  
= 0.294 $p_A$  + 0.105 $p_B$  + 0.601 $p_C$  [7]

According to Arita's assumptions, 19 which he calculated from another study carried in India, 24 the optimal distribution of vaccine priority should be based on the population without immunity:

$$m_A: m_B: m_C = (1-x-y): (1-v) \times : (1-\omega) y$$
  
; 69:17:14

where mA, mB, and mc are the ratio of the population who have not been immune based on residual immunity by Group A, B, and C. When we assume that the total amount of vaccines would be constant (for the purpose of comparison of immune population to be covered), we can transform these conditions into the ratio of proportion in need of vaccination by adjusting for the number in

each population as,

$$p_A: p_B: p_C; 86:9:5$$
 [9]

The conditions here are expressed as the proportion of people who needs to be vaccinated in each age group. Based on the equation [6], the optimal distribution of vaccine priority (the amount of vaccines) should be:

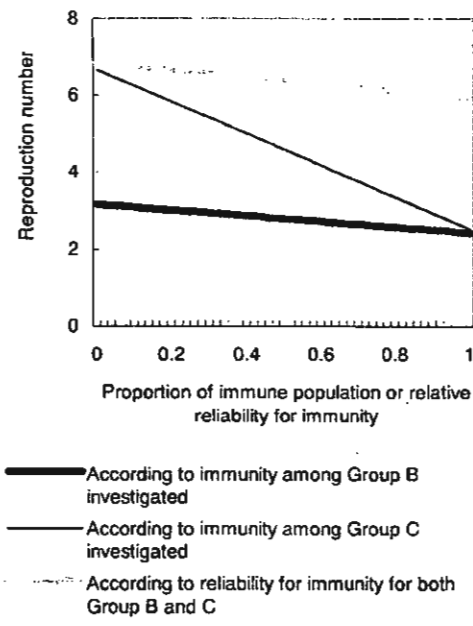
$$v_A: v_B: v_C; 84:4:12$$
 [10]

where  $v_A$ ,  $v_B$ , and  $v_C$  are the amount of vaccines needed by Group A, B, and C. Because we have set  $R_0 = 6.87$ , into eqn. [6] and [7], the minimum coverage and amount required to cause the small-pox epidemic to settle down in each age group is,

$$p_A \ge 74.21\%$$
  $v_A \ge 218,169$   
 $p_B \ge 2.65\%$   $v_B \ge 2,783$  [11]  
 $p_C \ge 8.59\%$   $v_C \ge 51,605$ 

The total amount of vaccination (V) should cover at least vA+vB+vC=272,557 persons in this scenario analysis. This can be calculated from:

$$V \ge v_A + v_B + v_C = \{ p_A (1 - x - y) + p_B x + p_C y \} N$$
 [12]



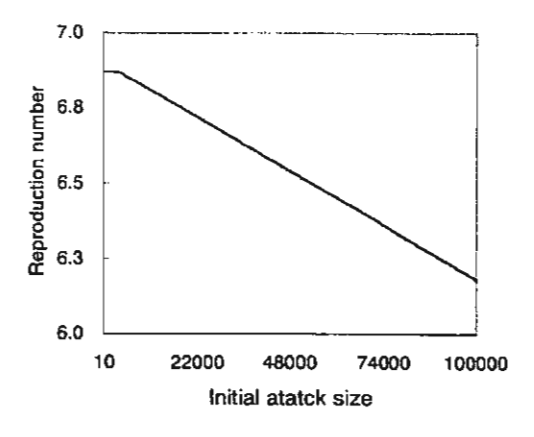


Figure 3. Sensitivity analysis for uncertain parameters.

The reproduction number under (a) varied proportion of the population with residual protective immunity as well as relative reliability for immunity among the population in Groups B (born in 1969-1977) and C (born before 1969), (b) different initial attack sizes from 10 to 100,000. The total population size was fixed at 10<sup>6</sup>.

Approximate coverage should be more than 27.3% of total population in our scenario analysis, while it would be necessary to cover 85.4% if we do not take immunity into account. If it becomes necessary to carry out nationwide mass-vaccination, we would need vaccines for between 27.3 and 85.4 million people depending on the different policies. Because the number does not take efficacy of the vaccine into account, the actual coverage might be greater than is given here.

Figure 3 shows the results of sensitivity analysis. The reproduction number changes linearly related to v,  $\omega$  and I(0)N. Comparing the proportion of the population possessing residual immunity between Group B and C, the reproduction number by varying Group B is more sensitive than C to the proportion of the immune population. Although the reproduction number increases as the relative reliability declines for both v and  $\omega$ , its increase seems rather small compared to drastic change in  $\omega$ . The reproduction number will also decline when initial attack size increases. However, compared to the change of the reproduction number on the order of 2.4 to 6.9 in Figure 3 (a), the varying interval in Figure 3 (b) is limited such as from 6.1 to 6.9

### DISCUSSION

Two important conclusions can be drawn from our assessments of the impact of immunity on possible smallpox epidemic in Japan. First, it demonstrates that the crude size of the potential epidemic could be greatly affected by the possible residual immunity within the population. Depending on the actual protective immunity, huge differences in smallpox incidence among the various population groups might be observed. Secondly, it is possible to determine how the optimal levels of vaccination should be when a nationwide vaccination becomes necessary, which is based on the immune status of the individuals. Therefore, if we could formulate a prioritization scheme for vaccination, which is based on the immunity of the individual, the total amount of vaccines could turn out to be much lower than the estimate given by the equal distribution policy.

Despite the problems of uncertainty with the real epidemiologic data of bioterrorism, a simple dynamic model still gave reasonable simulations of the smallpox dynamics. Because transmission potential varies from community to community, we performed a sensitivity analysis according to the residual immunity and initial attack size for determined Ro, which was within the range of precise estimate. Because initial attack size itself does not largely affect the transmission potential, the size of epidemic would be linearly increase according to the initial attack size in further simulations based on our assumption (mostly it originates from assuming homogenous mixing). Although the results of a longlasting protective effects of smallpox vaccination is still based on theoretical analysis25 with certain assumptions, the impact of residual immunity on the size of epidemic can clearly be demonstrated when we examine the natural course of epidemic (without any interventions). Because mass-vaccination measures greatly

affect the transmissibility, the rapidity with which the smallpox epidemic spread would largely be lessened by the presence of the residual immunity. The national policy to achieve optimal distribution of vaccination should therefore be formulated on the basis of residual immunity among its population. This might affect the longevity of the epidemic as well as how fast it spreads. The contribution of residual immunity to the probability of controlling smallpox outbreak can be described by equation [6]. It might be possible to estimate the total amount of vaccines needed (equation [12]) when smallpox begins to spread into each community. The model has also been generalized so that it can be used to achieve the estimation for other communities. The minimum amount of vaccines that needs to be stocked in order to obtain herd immunity (or eradicate) against smallpox would be 3.13 times lesser than the amount needed when no immunity exists. According to sensitivity analysis, the possible trajectories would be sensitive to the proportion of immune population in Group C. It is considered to be due to the large number of the population in Group C. The overall number of vaccine doses would be an underestimate because efficacy of the vaccine must also be taken into account if a mass-vaccination was to take place.

Although our study demonstrates the large impact of residual immunity on the epidemic, the real percentage and duration of immunity are unknown. Our study is based on certain assumptions. It is therefore critically important to know the status of immunity in the real population from epidemiologic studies. In this study, we considered the impact of varying residual immunity in each age group by looking at the sensitivity of associated parameters ( v and  $\omega$  being the most critical). Such sensitivity analyses can help estimating the variability in the size of epidemic and the reproduction number. One should also note that mass vaccination before a bioterrorist attack actually takes place is not practicable in the real settings. Although we focused on the impact of residual immunity and its application for calculating required stock for vaccination as a possible implication, vaccination would start after an identification of the attack. There would be a race of time between implementing of vaccination and the spread of transmission. 12.26 For the purpose of practical planning or simulation, it would be necessary to consider these important aspects.

Our study has several limitations, however. Much needs to be overcome in order to increase model realism. First, one of the major problems, which the world must confront, is the uncertainty and lack of knowledge on smallpox bioterrorism. We believe that one approach to overcome the problem of risk management is to model the potential episodes with mathematical modeling. This study was conducted with only a few known parameter values, and our method assumed a closed population with crude results (in addition, simulations without quarantine). Although we assumed the introduction of smallpox into an urban community, epidemic could be different between urban and rural communities because population density as well as many of the socio-demographic and behavioral characteristics vary. Thus there are many uncertainties. It should be noted that many other variables could

affect the course of epidemic in real world bioterrorism such as the pattern of contacts. Although we assumed homogenous mixing within the community, the spread in scale-free networks should further be considered, and intercommunity migration should also be taken into account. Secondly, the estimation of total amount of vaccine needed is based on optimistic assumption. We do not know the actual percentage of residual immunity and the vaccine efficacy. We need further epidemiologic studies on immunity as well as on vaccine trials for smallpox. Finally, although possible outcomes were determined for a certain population size, one should not expect the same outcome for cities of the same size because of regional variances in the age distribution. Since the formula for the total amount of vaccination needed has been generalized, each community should be able to calculate the requirements based on their own epidemiologic records and age distributions. In order to prepare the various communities, including ours, for future possible bioterrorist attacks as well as to facilitate the use of mathematical models in policy formulation, we open ourselves to criticisms, comments and suggestions for collaborations with others academic who share the same concern.

### **ACKNOWLEDGEMENTS**

This work was mainly carried out while HN was staying in Thailand. Thanks are due to Professor Masayuki Kakehashi at Institute of Health Sciences, Hiroshima University for his technical advice and comments. Thanks are also due to Dr Isao Arita at Agency for Cooperation in International Health for his suggestions and critical opinions. We are grateful to Ms. Lisa Imadzu, Dr Hideki Yanai (both at The Research Institute of Tuberculosis, Japan), and reviewers of editorial board for their critical review and suggestion for improvement. HN is also grateful to the Showa Ikeda Memorial Foundation for supporting his stay in Thailand.

### REFERENCES

- Hughes JM. The emerging threat of bioterrorism. Emerg Infect Dis 1999;5:494-5.
- Henderson DA, Inglesby TV, Bartlett JG, Ascher MS, Eitzen E, Jahrling PB et al. Smallpox as a biological weapon: medical and public health management. Working Group on Civilian Biodefense. JAMA 1999;281:2127-37.
- Fenner F, Henderson DA, Arita I, Jezek Z, Ladnyi ID. Smallpox and its eradication. World Health Organization, Geneva, 1988 (Available at: http://www.who.int/emc/diseases/smallpox/Smallpoxeradication.html).
- Anonymus. US sounds alarm over smallpox weapon threat. Nature 1999;399:628.
- Centers for Disease Control. CDC Interim Smallpox Response Plan and Guidelines. Centers for Disease Control, Atlanta, 2002.
- Holloway HC, Norwood AE, Fullerton CS, Engel CC, Jr., Ursano RJ. The threat of biological weapons. Prophylaxis

- and mitigation of psychological and social consequences. JAMA 1997;278:425-7.
- Council on Foreign Relations. Terrorism Q&A: Japan. Council on Foreigin Relations, New York, 2002.
- Jernigan JA, Stephens DS, Ashford DA, Omenaca C, Topiel MS, Galbraith M, et al. Bioterrorism-related inhalational anthrax: the first 10 cases reported in the United States. Emerg Infect Dis 2001;7:933-44.
- Anonymus. Domestic production of smallpox vaccines; developed 20 years ago. Kyodo Press. 28th July. (In Japanese), 2003.
- Ministry of Health, Labor and Welfare. Response plan for domestic biological warfare. Ministry of Health, Labor and Welfare, Tokyo, 2003. (In Japanese)
- Meltzer MI, Damon I, LeDuc JW, Millar JD. Modeling potential responses to smallpox as a bioterrorist weapon. Emerg Infect Dis 2001;7:959-69.
- Kaplan EH, Craft DL, Wein LM. Emergency response to a smallpox attack: the case for mass vaccination. Proc Natl Acad Sci U S A 2002;99:10935-40.
- Bozzette SA, Boer R, Bhatnagar V, Brower JL, Keeler EB, Morton SC, et al. A model for a smallpox-vaccination policy. N Eng J Med 2003;348:416-25.
- Eichner M. Case isolation and contact tracing can prevent the spread of smallpox. Am J Epidemiol 2003;158:118-28.
- Gani R, Leach S. Transmission potential of smallpox in contemporary populations. Nature 2001;414:748-51.
- Eichner M, Dietz K. Transmission potential of smallpox: estimates based on detailed data from an outbreak. Am J Epidemiol 2003;158:110-7.
- Blower SM, Medley GF. Epidemiology, HIV and drugs: mathematical models and data. Br J Addict 1992;87:371-9.
- Banks T, Castillo-Chavez C. Mathematical and Modeling Approaches in Homeland Security. SIAM's, Frontiers in Applied Mathematics, New York, 2003.
- Arita I. Duration of immunity after smallpox vaccination: a study on vaccination policy against smallpox bioterrorism in Japan. Jpn J Infect Dis 2002; 55: 112-6.
- Henderson DA, Moss B. Smallpox and vaccinia. In Plotkin SA, Orenstein WA, Offit PA, eds. Vaccines, 4th eds. Elsevier Science, New York. 2003: Chapter 6 (3rd eds available at http://www.ncbi.nlm.nih.gov/books/bv.fcgi?call=bv.View..Sh owSection&r id=vacc.chapter.3)
- Anderson RM, May RM. Infectious Diseases of Humans: Dynamics and Control. Oxford University Press, Oxford, 1991.
- Diekmann O, Heesterbeek JAP. Mathematical Epidemiology of Infectious Diseases: Model Building, Analysis and Interpretation. Wiley, New York, 2000.
- Kaplan EH. Mean-max bounds for worst-case endemic mixing models. Math Biosci 1991;105:97-109.
- 24. Rao AR. Smallpox. Kothari Book Dept., Bombay, 1972.
- 25. Eichner M. Analysis of historical data suggests long-lasting

H, et al. 49

protective effects of smallpox vaccination. Am J Epidemiol 2003;158:717-23.

- Ferguson NM, Keeling MJ, Edmunds WJ, Gani R, Grenfell BT, Anderson RM, et al. Planning for smallpox outbreaks. Nature 2003;425:681-5.
- Gelfand HM, Posch J. The recent outbreak of smallpox in Meschede, West Germany. Am J Epidemiol 1971;94:234-7.
- 28. Mack TM. Smallpox in Europe, 1950-1971. J Infect Dis 1972;125:161-9.
- Chowell G, Fenimore PW, Castillo-Garsow MA, Castillo-Chavez C. SARS outbreaks in Ontario, Hong Kong and Singapore: the role of diagnosis and isolation as a control mechanism. J Theor Biol 2003;224:1-8.
- 30. Iwasaki M, Otani T, Ohta A, Yosiaki S, Kuroiwa M, Suzuki S. Rural-urban differences in sociodemographic, social network and lifestyle factors related to mortality of middle-aged Japanese men from the Komo-Ise cohort study. J Epidemiol 2002;12:93-104.

### **APPENDIX**

For the purpose of further realistic simulation, here we consider the effect of quarantine onto our model (using additional five compartments, Figure 4). We suppose the fraction q, of those who are known to have been exposed and therefore may be infected but are not yet ill, would be quarantined (denoted by the compartment  $E_q$ ). Those who are in  $E_q$  will become infectious after the latency period (and enter into  $I_q$ ). Some of them would be diagnosed and moved into isolation with the mean daily rate  $\delta$  (and enter into J). The other of infectious and traced individuals are assumed to recover or die after ( $\gamma$ ) days of quarantine. In addition to quarantining the infected individuals, we need to consider uninfected and traced individuals. Among uninfected,  $(I-q)(I-\beta)$  remains susceptible and  $q(I-\beta)$  would be traced and enters into

Qs, Qg and Qc: which represent those who are traced but uninfected for each age group. Those who were traced but uninfected would finish quarantine (released into community again and enter the susceptible population)  $\sigma^{-1}$  days after their known contact. Since we should assume the quarantine can never be perfect to protect an additional transmission, relative measure of reduced risk among those quarantined ( $\theta$ ) is multiplied to  $I_q$ . Incorporating these assumptions onto equations [1], the transmission dynamics with the modification of quarantine system can be described to

$$\frac{dS_A}{dt} = -\zeta (1 - p_A) \{q + \beta (1 - q)\} S_A (I + \theta I_q + \pi J) + \sigma Q_A$$

$$\frac{dS_B}{dt} = -\zeta (1 - v - p_B) \{q + \beta (1 - q)\} S_B (I + \theta I_q + \pi J) + \sigma Q_B$$

$$\frac{dS_C}{dt} = -\zeta (1 - v - p_C) \{q + \beta (1 - q)\} S_C (I + \theta I_q + \pi J) + \sigma Q_C$$

$$\frac{dQ_A}{dt} = (1 - p_A) (1 - \beta) \zeta qS_A (I + \theta I_q + \pi J) - \sigma Q_A$$

$$\frac{dQ_B}{dt} = (1 - v - p_B) (1 - \beta) \zeta qS_B (I + \theta I_q + \pi J) - \sigma Q_B$$

$$\frac{dQ_C}{dt} = (1 - \omega - p_C) (1 - \beta) \zeta qS_C (I + \theta I_q + \pi J) - \sigma Q_C$$

$$\frac{dE_q}{dt} = \beta \zeta q \{(1 - p_A)S_A + (1 - v - p_B)S_B + (1 - \omega - p_C)S_C\} (I + \theta I_q + \pi J) - \phi E_q$$

$$\frac{dE}{dt} = \beta \zeta (1 - q) \{(1 - p_A)S_A + (1 - v - p_B)S_B + (1 - \omega - p_C)S_C\} (I + \theta I_q + \pi J) - \phi E_q$$

$$\frac{dI_q}{dt} = \phi E_q - (\gamma_3 + \delta)I_q$$

$$\frac{dI_q}{dt} = \phi E - (\gamma_1 + \delta)I$$

$$\frac{dJ}{dt} = \delta (I + I_q) - \gamma_2 J$$

$$\frac{dR}{dt} = \gamma_1 I + \gamma_2 J - \gamma_3 I_q$$

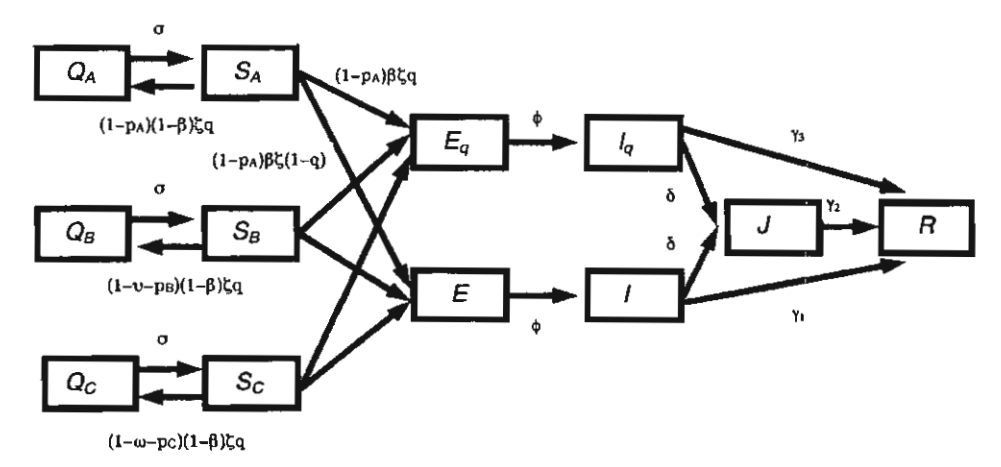


Figure 4. The transmission dynamics of the smallpox incorporating the effect of quarantine.

Additional compartments:  $E_q$  represents the proportion of traced latent contacts;  $Q_A$ ,  $Q_B$  and  $Q_C$ , the proportion of traced uninfected contacts from Groups A (born after 1977), B (born in 1969-1977), and C (born before 1969);  $I_q$  the proportion of infectious in quarantine.

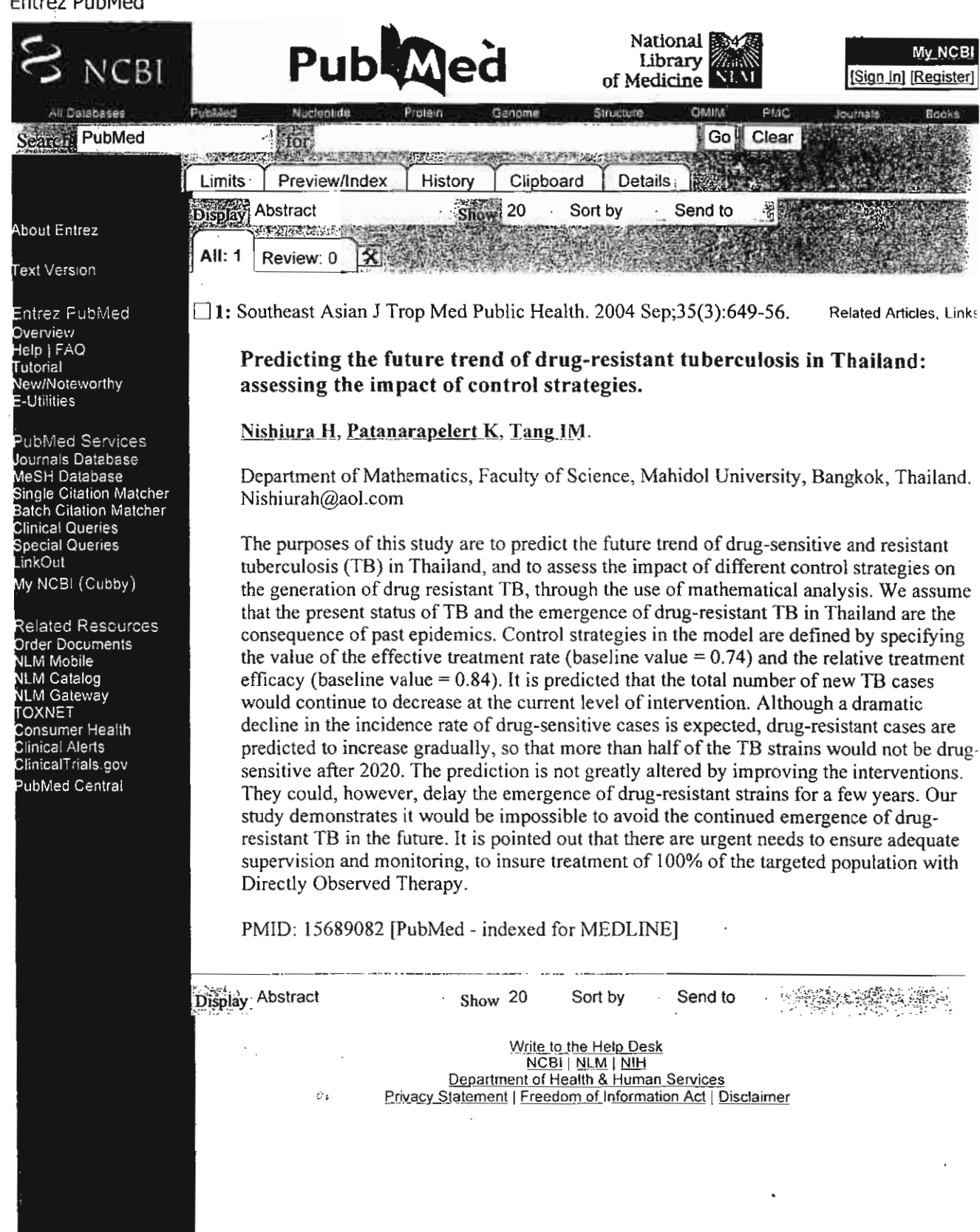
In this case, the basic reproduction number would be given by

$$R_{0} = \zeta \beta (1-q) N \{ (1-p_{A}) (1-x-y) + (1-v-p_{B})x + (1+\omega-p_{C})y \}$$

$$\times \left\{ \frac{1}{\delta + \gamma_{1}} + \frac{\theta}{\delta + \gamma_{3}} + \frac{\delta \pi}{\gamma_{2}(\delta + \gamma_{1})} \right\}$$
[2']

This would allow to increase the realism for simulation.

### Entrez PubMed





ą

ScienceAsia 31 (2005): 193-199

### Limit Cycle in a Herbivore-Plant-Bee Model Containing a Time Delay

Charoen Kaewpradit, Wannapong Triampob and I-Ming Tangbe.

- Openation of Mathematics
- Department of Physics and Capability Building Unit in NanoScience & NanoTechnology Faculty of Science, Mahido! University, Bangkok 10400, Thailand
- c Institute of Science & Technology for Research & Development Mahidol University, Nakhon Pathorn 73170, Thalland
- \*Corresponding author: e-mail address scimt@mahidol.ac.th

Received 28 Jul 2004 Accepted 23 Mar 2005

**ABSTRACT:** The dynamical behavior of time delay herbivore-plant-pollinator ecosystem is studied. The time delay arises from the fact that it takes time for a pollinated flower to develop into a new plant. A dynamical analysis is used to show that a stable steady state undergoes a Hopf bifurcation to a limit cycle behavior as the delay time crosses a critical value. This prediction is verified by numerically solving the set of first order differential equations. One finds that the trajectory which is spiraling into the steady state point when  $\tau < \tau_o$  becomes a trajectory into a limit cycle about the state when  $\tau > \tau_c$ .

KEYWORDS: Herbivore-plant-pollinator ecosystem, time delay, Hopf Bifurcation.

### INTRODUCTION

Very recently, Bandyopadhyay, Bhattacharyya and Mukopadhyay (BBM)1, studied the dynamics of an autotroph-herbivore ecosystem with nutrient recycling. They considered both the case where there is no time delay and the case where there is a delay. For the former case, they found that when the rate of increase of the nutrients attained a certain threshold value, the system became stable. The autotroph and herbivore populations would oscillate about an interior steady state point. Below the threshold value, the system became unstable. Note that in the absence of nutrient replenishing, the nutrients would eventually disappear from the soil and the autotrophic state would go to zero. For the latter case, BBM found that a sufficiently large delay in the time needed to convert dead organic matter into the nutrients, would cause the stable state to become unstable. Using Hopf Bifurcation analysis<sup>2</sup>, they established the conditions for the switching of the stability.

Jang<sup>3</sup> has studied the dynamics of a herbivore-plant-pollinator ecosystem. Jang's model is somewhat different from that of BBM. He looked at the roles of the energetic rewards of the interactions between the plant and the pollinator and of the specificity of the pollinator to the plant. Jang was particularly interested in how the reduction of the visitation rate of the bee to the plant caused by the action of the herbivore affected

the ecosystem. A Hopf Bifurcation analysis was again used to determine the stability of the steady states. Jang did not include any time delay<sup>4,5</sup> into his model.

The purpose of the present paper is to determine the effects of a time delay in Jang's model. Unlike the BBM model, where the time delay should be inserted is obvious, it is not in Jang's model. We believe that it should be inserted into the term describing the birth rate of the plant;

$$\frac{k_1 \sigma \mu XY}{1 + \sigma \phi \mu^2 Y} \tag{1}$$

where X and Y are the bee and plant populations, respectively;  $k_1$ , number of ovules fertilized per visit of the bee;  $\sigma$ , the probability of an encounter between the flower and the bee;  $\phi$ , reciprocal of the time it takes the bee to extract the nectar (or pollen); and  $\mu$ , the energetic reward to the bee when it encounters the flower. This gives the number of flowers fertilized at time t. It then takes time for the fertilized ovules to develop into seeds and fall to the ground. The number of new plants that will begin to flower at time t will depend on the number of ovules that were fertilized at time t- $\tau$ , where  $\tau$  is the time delay. In Section II, we introduce the Jang model and present some of his results. We put the time delay into the model in Section III, and carry out a Hopf Bifurcation analysis. In Section IV, we present our

numerical solution. In Section V, we present an extension of our model and discuss how it can be used to provide quantitative predictions for the farmers.

### II. Jang's Model.

The herbivore-plant-pollinator ecosystem considered by Jang consists of three first order differential equations;

$$X = bX(K - X) + \frac{g(Z)k_2\sigma\mu^2XY}{1 + \phi\sigma\mu^2Y}$$
(2a)  

$$Y = \frac{k_1\sigma\mu g(Z)XY}{1 + \phi\sigma\mu^2Y} - \gamma Y - \frac{m_1YZ}{a + Y}$$
(2b)

$$\dot{Y} = \frac{h_1 \sigma \mu g(Z) X Y}{1 + 4 \sigma \mu^2 Y} - \gamma Y - \frac{m_1 Y Z}{\sigma + Y}$$
 (2b)

and

$$\dot{Z} = \frac{m_2 YZ}{a + Y} - \delta Z \tag{2c}$$

where Z denotes the herbivore population; g(z) represents the loss in attractiveness of the flower to the bee due to the damage caused by the herbivore;

$$\frac{m_2 Y}{a + Y} \tag{3}$$

is the visitation rate of the herbivore to the plant; m, and m, the maximal ingestion rate and the leafhopper maximal growth rate with 0 < m, ≤ m, respectively; 'a', the half - saturation constant;  $\delta_1$ , the maximum per capita birth rate of the bees;  $\lambda$  and  $\delta$ , the death rate of the bees and herbivore, respectively; 'b', the density dependent regulation constant of bee, and K is the measure of the diversity of bee to the plant  $(K=(\delta_1-\lambda)/$ b). In the present model, the flower on the plant becomes pollinated and after awhile, the plant dies. The life cycle begins again when the seed developed from the pollinated flower falls off the plant and germinates in the soil. All of the population classes must be positive at all times, i.e.,

$$X(t), Y(t), Z(t)^3 \ge 0$$
.

Setting the RHS of eqns. (2a) - (2c) to zero, we obtained

m, 
$$\overline{x} = K + \frac{g(\overline{z})k_1\mu^2\sigma\overline{y}}{b(1+\phi\sigma\mu^2\overline{y})}$$
 (4a)

$$\overline{y} = \frac{a\delta}{m - \delta}, m_2 > \delta$$
 (4b)

$$\bar{z} = \frac{a + \bar{y}}{m_1} \left[ \frac{k_1 k_2 \mu^3 o^2 \bar{y}}{b(1 + \phi o \mu^2 \bar{y})^2} g(\bar{z})^2 + \frac{k_1 \mu o K}{1 + \phi o \mu^2 \bar{y}} g(\bar{z}) - \gamma l (4c) \right]$$

at one of the steady states  $(\bar{x}, \bar{y}, \bar{z})$ . To determine when the state is stable or not, we first diagonalize the Jacobian of eqns. (2a) to (2c) at the steady state. We then check to see if all the eigenvalues have negative real parts. When this happens, the state is stable. Diagonalizing the Jacobian, we obtain the following characteristic equation

$$\lambda^{3} + (p_{1} - s_{1})\lambda^{2} + (p_{2} - s_{2})\lambda + (p_{3} - s_{3}) = 0$$
 (5)

$$p_1 = \gamma + \delta - bK + 2b\overline{x} - m_2h(\overline{y}) - k_2\mu f(\overline{y})g(\overline{z}) + m_1\overline{z}h'(\overline{y}),$$

$$\begin{split} p_2 &= \gamma \delta - b K \delta - b K \gamma + 2 b \gamma \overline{x} + b K h(\overline{y}) m_1 - \gamma h(\overline{y}) m_2 - 2 b h(\overline{y}) \overline{x} m_2 \\ &+ 2 b \delta \overline{x} - \gamma f(\overline{y}) k_2 \mu g(\overline{z}) - \delta f(\overline{y}) k_2 \mu g(\overline{z}) + f(\overline{y}) h(\overline{y}) k_2 m_2 \mu g(\overline{z}) \\ &- b K \overline{z} m_1 h'(\overline{y}) + \delta \overline{z} m_1 h'(\overline{y}) + 2 b \overline{x} \overline{z} m_1 h'(\overline{y}) - f(\overline{y}) \overline{z} \ k_2 m_1 \mu g(\overline{z}) h'(\overline{y}), \end{split}$$

$$\begin{split} p_3 &= 2b\gamma\delta\overline{\mathbf{x}} - bK\gamma\delta + bK\gamma h(\overline{\mathbf{y}}) m_{\gamma} - 2b\gamma h(\overline{\mathbf{y}})\overline{\mathbf{x}} m_{\gamma} - \gamma\delta h(\overline{\mathbf{y}})k_{\gamma}\mu g(\overline{\mathbf{z}}) \\ &+ \gamma f(\overline{\mathbf{y}})h(\overline{\mathbf{y}})k_{\gamma}m_{\gamma}\mu g(\overline{\mathbf{z}}) - bK\delta\overline{\mathbf{z}} m_{\gamma}h'(\overline{\mathbf{y}}) + 2b\delta \quad \overline{\mathbf{x}}\overline{\mathbf{z}} m_{\gamma}h'(\overline{\mathbf{y}}) \\ &- \delta f(\overline{\mathbf{y}})\overline{\mathbf{z}}k_{\gamma}m_{\gamma}\mu g(\overline{\mathbf{z}})h'(\overline{\mathbf{y}}), \end{split}$$

 $s_1 = g(\overline{z})\overline{x} k_1 f'(\overline{y}),$ 

$$s_1 = -bKg(\overline{z})\overline{x}k_1f'(\overline{y}) + \delta g(\overline{z})\overline{x} \ k_1f'(\overline{y}) + 2bg(\overline{z})\overline{x}^2k_1f'(\overline{y}) -g(\overline{z})h(\overline{y})\overline{x} \ k_1m_2f'(\overline{y}) + f(\overline{y})\overline{x} \ \overline{z}k_1m_2g'(\overline{z})h'(\overline{y})$$

$$\begin{split} s_3 &= 2b\delta g(\overline{z})\overline{x}'k_1f'(\overline{y}) - bK\delta g(\overline{z})\overline{x}k_1f'(\overline{y}) + 2b\ f(\overline{y})\ \overline{x}^2\ \overline{z}\ k_1m_2g'(\overline{z})\ h'(\overline{y}) \\ &+ bK\ g(\overline{z})\ h(\overline{y})\ \overline{x}\ k_1m_2\ f(\overline{y}) - 2b\ g(\overline{z})\ h(\overline{y})\ \overline{x}^2k_1m_2\ f'(\overline{y}) \\ &- bK\ f(\overline{y})\ \overline{x}\ \overline{z}\ k_1m_2\ g'(\overline{z})\ h'(\overline{y}) \end{split} \tag{6}$$

Equation (5) has negative real roots if and only if (Theorem 1, Appendix)

$$P_1-S_1>0$$
,  $P_3-S_3>0$  and  $(P_1-S_1)(P_2-S_2)-(P_3-S_3)>0$ . (7)

When the above conditions are satisfied  $(\bar{x}, \bar{y}, \bar{z})$ , the steady state will be stable.

### III.Effect of Time Delay. Illa. The Stability of $\overline{E} = (\overline{x}, \overline{y}, \overline{z})$ with Time Delay.

A time delay in the herbivore-plant-pollinator system arises because a new flower only arrives after the pollinated flower develops into a seed, falls off the plant, germinates into a new plant and then grows into the flowering stage of the new plant. To include the effects of the time delay, we need to replace eqn. (2b)

$$\dot{y} = \frac{k_1 \mu \sigma g(z(t-\tau))x(t-\tau)y(t-\tau)}{1+\phi \sigma \mu^2 y(t-\tau)} \quad \gamma y \quad \frac{m_1 yz}{a+y} \quad (2b')$$

The Jacobian matrix for eqns. (2a), (2b') and 2c) evaluated at the steady state point  $\overline{E} = (\overline{x}, \overline{y}, \overline{z})$  is

$$\begin{pmatrix} bK - 2b\bar{x} + k_2 \ \mu g(\bar{z} \ ) \ f(\bar{y}) & k_2 \ \mu g(\bar{z}) \ f'(\bar{y}) \ \bar{x} \\ k_1 \ g(\bar{z}) \ f(\bar{y}) \ e^{-i\omega\tau} & -\gamma - m_1 \ \bar{z} & h'(\bar{y}) + k_1 \ g(\bar{z}) \ \bar{x} \ f'(\bar{y}) \ e^{-i\omega\tau} \\ 0 & m_2 \ \bar{z} & h'(\bar{y}) \end{pmatrix}$$

$$\begin{array}{c} k_{2}\mu g'\left(\overline{z}\right)f(\overline{y})\,\overline{x}\\ -m_{1}\,h(\overline{y}\,\,)+k_{1}\,g'(\overline{z}\,\,)\,\overline{x}\,\,f(\overline{y}\,\,)\,e^{-\omega\tau}\\ m_{2}\,\,h(\overline{y})-\delta \end{array} \right) \end{(8)}$$

Diagonalizing the above matrix, we obtain the following characteristic equation<sup>5</sup>

$$\omega^3 + p_1 \omega^2 + p_2 \omega + p_3 = e^{-\omega \tau} (s_1 \omega^2 + s_2 \omega + s_3)$$
 (9)

We now suppose that two of the eigenvalues of eqn. (9) are a pair of complex conjugates

i.e.,  $\omega_{\pm} = u(\tau) \pm iv(\tau)$ . Substituting  $\omega_{+}$  into eqn. (9) and separating the real and imaginary parts, we get

$$u^{3} - 3uv^{2} + p_{1}u^{2} - p_{1}v^{2} + p_{2}u + p_{3}$$

$$= e^{-u\tau} \{s_{1}u^{2}\cos(v\tau) - s_{1}v^{2}\cos(v\tau) + s_{2}u\cos(v\tau) + s_{3}\cos(v\tau)\}$$

$$+2s_{1}uv\sin(v\tau) + s_{2}v\sin(v\tau)$$
(10)

and

3

4

$$3u^{2}v - v^{3} + 2p_{1}uv + p_{2}v$$

$$\stackrel{\parallel}{=} e^{-u\tau} \{2s_{1}uv \cos(v\tau) + s_{2}v \cos(v\tau) - s_{1}u^{2} \sin(v\tau) + s_{1}v^{2} \sin(v\tau) - s_{2}u \sin(v\tau) - s_{3}\sin(v\tau)\}$$
(11)

where  $\tau$  is chosen to be the Hopf bifurcation parameter.

For a Hopf bifurcation to occur, three conditions must be met at the critical value  $(\tau_o)$ ;  $(1)u(\tau_o) = 0$ ,  $(2)v(\tau_o) \neq 0$  and  $(3)u'(\tau_o) > 0$  (Theorem 2, Appendix). To see if the eigenvalues of the Jacobian evaluated at the steady state point  $\overline{E} = (\overline{x}, \overline{y}, \overline{z})$  satisfy these conditions, we first assume that the critical value defined by  $u(\tau_o) = 0$  exist. However, we do not use this condition to find  $\tau_o$ . Instead we substitute the condition into eqns. (10) and (11) and see whether a non-zero value of  $v(\tau_o)$  exist. To do this, we set  $u(\tau_o) = u^* = 0$  into the two equations to get

$$-p_1 v^{*2} + p_3 = (s_3 - s_1 v^{*2}) \cos(v^* \tau_0) + s_2 v^* \sin(v^* \tau_0)$$
(12)

$$-v^{*3} + p_2 v^* = s_2 v^* \cos(v^* \tau_0) - (s_3 - s_1 v^{*2}) \sin(v^* \tau_0)$$
 (13)

Squaring the two equations and adding the squares together, we obtain

$$v^{*6} + (p_1^2 - 2p_2 - s_1^2)v^{*4} + (p_2^2 - 2p_1p_3 - s_2^2 + 2s_1s_3)v^{*2} + (p_3^2 - s_3^2) = 0$$
(14)

Letting  $v^{2}$ ,  $\eta$  eqn. (14) becomes the following cubic equation

$$S(\eta) = \eta^3 + d_1 \eta^2 + d_2 \eta + d_3 = 0$$
 (15)

where

$$d_1 = p_1^2 - 2p_2 - s_1^2 (16a)$$

$$d_2 = p_2^2 - 2p_1p_3 - s_2^2 + 2s_1s_3 \qquad (16b)$$

$$d_3 = p_3^2 - s_3^2 \tag{16c}$$

For  $v(\tau_n)$  to exist, the roots of eqn. (15) must be real and

positive. This can be determined by using the results of the lemma stated in the Appendix. We now assume that a set of values for the parameters can be found which satisfies the conditions of Lemma 1.

Next we need to show that for the present  $u(\tau)$ , the following is true

$$\frac{\mathrm{d}\mathbf{u}}{\mathrm{d}\tau}\bigg|_{\tau=\tau_0} > 0 \tag{17}$$

This is done by differentiating eqns. (10) and (11) with respect to  $\tau$  and then set  $\tau = \tau$ . Doing this, we get

$$B\frac{\mathrm{d}u}{\mathrm{d}\tau}\Big|_{\tau=\tau_0} + C\frac{\mathrm{d}v}{\mathrm{d}\tau}\Big|_{\tau=\tau_0} = D \qquad (18a)$$

$$-C\frac{\mathrm{d}u}{\mathrm{d}\tau}\Big|_{\tau=\tau_0} + B\frac{\mathrm{d}v}{\mathrm{d}\tau}\Big|_{\tau=\tau_0} = E \qquad (18b)$$

where

$$B = \begin{bmatrix} -3v_0^2 + p_2 - s_2\cos(v_0\tau_0) - 2s_1v_0\sin(v_0\tau_0) + s_3\tau_0\cos(v_0\tau_0) \\ -s_1v_0^2\tau_0\cos(v_0\tau_0) + s_2v_0\tau_0\sin(v_0\tau_0) \end{bmatrix}$$

$$C = \left[ -2p_1 v_0 + 2s_1 v_0 \cos(v_0 t_0) + s_3 \tau_0 \sin(v_0 t_0) - s_1 v_0^2 \tau_0 \sin(v_0 \tau_0) - s_2 \sin(v_0 \tau_0) - s_2 v_0 t_0 \cos(v_0 \tau_0) \right]$$

$$D = (s_1 v_0^3 - s_3 v_0) \sin(v_0 \tau_0) + s_2 v_0^2 \cos(v_0 \tau_0)$$
and

$$E = (s_1 v_0^3 - s_3 v_0) \cos(v_0 \tau_0) - s_2 v_0^2 \sin(v_0 \tau_0)$$
 (19)

Solving for 
$$\frac{du}{d\tau}\Big|_{\tau=\tau_0}$$
 we get
$$\frac{du}{d\tau}\Big|_{\tau=\tau_0} = \frac{BD - EC}{B^2 + C^2}$$
 (20)

where

BD-EC = 
$$v_0^2 [3v_0^4 + 2v_0^2(p_1^2 - 2p_2 - s_1^2) + (p_2^2 - 2p_1p_3 - s_2^2 + 2s_1s_3)]$$
(21)

Therefore, we have

$$\frac{du}{d\tau}\bigg|_{\tau=\tau_0} = \frac{v_0^2}{g^2 + C^2} \{3v_0^4 + 2v_0^2(p_1^2 - 2p_2 - s_1^2) + (p_2^2 - 2p_1p_3 - s_2^2 + 2s_1s_3)\}$$
Noting that

$$\frac{dS}{d\eta} = 3\eta^2 + 2(p_1^2 - 2p_2 - s_1^2)\eta + (p_2^2 - 2p_1p_3 - s_2^2 + 2s_1s_3)$$

where S is defined by eqn. (15), eqn. (22) can be written as

$$\frac{du}{d\tau}\Big|_{\tau=\tau_0} = \frac{v_0^2}{B^2 + C^2} \frac{dS}{d\eta}\Big|_{\eta=v_0^2}$$
 (24)

The condition  $\Delta < 0$  in part A of Lemma I requires the two turning points of  $S(\eta)$  not be a positive real root of  $S(\eta)$ , otherwise  $\Delta$  would be equal to zero. The two turning points of  $S(\eta)$ ,  $\epsilon_1$  and  $\epsilon_2$  (eqn. A2), are the zeros of eqn. (23). Since  $v_0^2 \neq {}^1 \epsilon_{12}$ , the following must be true

$$\frac{dS}{d\eta}\Big|_{\eta=v_0^2} \neq 0 \tag{25}$$

Thus

$$\frac{du}{d\tau}\Big|_{\tau=\tau_0} = \frac{v_0^2}{B^2 + C^2} \frac{dS}{d\eta}\Big|_{\eta=v_0^2}$$
 (26)

and condition 3 of the Hopf bifurcation theory is satisfied. Therefore the system undergoes a Hopf bifurcation.

### IIIb.Critical Time Delay.

The critical delay time can be found by using the method introduced by Tam.<sup>6</sup> We rewrite eqns (12) and (13) as

$$M\cos(v * \tau_0) + N\sin(v * \tau_0) = P$$
 (27a)

$$N\cos(v * \tau_0) - M\sin(v * \tau_0) = Q \qquad (27b)$$

where

$$M = S_3 - S_1 V^{*2} (28a)$$

$$N = S_2 V^* \tag{28b}$$

$$P = -P_1 V^{*2} + P_3 (28c)^{-1}$$

and

$$Q = -V^{*3} + P_2 V^*$$
 (28d)

Eqns. (27a) and (27b) leads to

$$M^2 + N^2 = P^2 + Q^2 = G^2$$
, where  $G > 0$ . (29)

M and N can be rewritten as

$$M = G \cos \theta$$

$$N = G \sin \theta$$
 (30)

This allows us to determine  $a\theta \in [0, 2\pi)$  uniquely. With this value of  $\theta$ , eqns. (27a) and (28b) become

$$G\cos(\tau_0 v^*)\cos\theta + G\sin(\tau_0 v)\sin\theta = P$$
 (31)

$$G\cos(\tau_0 v *)\sin\theta - G\sin(\tau_0 v *)\cos\theta = Q \qquad (32)$$

or

$$G\cos(\tau_{o}v * - \theta) = P$$
 (33a)

$$G\sin(\tau_0 \mathbf{v} * - \theta) = Q \tag{33b}$$

From this we get as the critical value

$$\tau_0 = \frac{1}{r} \{ \tan^{-1}(\frac{Q}{P}) + \theta \}$$
 (34)

### IV. Numerical Solution.

### IVa. Numerical Parameters.

The numerical values of the parameters in the herbivore-plant-pollinator ecosystem for a given plant are scarce. One has to guess at them since many of them will depend on which plant we are interested in, what is the locality (or country) or what time of the year it is. To gain ideas of the range of values the parameters can take, we look at the Mango tree, even though the present model is not an appropriate model for this plant. The model is developed for a flowering plant which after becoming pollinated, dies. Most Mango trees exhibit biannual flowering, once between May and June and again in December-January. This flowering is repeated every year for many years. Nevertheless, we have used the data available for the Mango trees to be typical of most plants.

Jamjanya<sup>7</sup> has looked at the increase in leafhopper population in two varieties of mango trees, On-som and Na thub. He found that leafhopper infestation on the Na-thub mango tree increased by 270% in a day, while the leafhoppers infestation on the On-sorn mango tree increased 63% in a day. This implies that m, can vary between 0.63 - 2.7 day-1 depending on the type of Mango tree. Boongird8 has measured the probability that a bee will visit a Nam dok mai mango tree in Thailand. He found  $\sigma$  to be 79.55%. In Trinidad, the probability that a bee will visit the mango is about 21%.9 We take  $\sigma$ , the probability of encounter to be in the range 0.21 - 1.0. The extraction rate of the nectar by the bee range between 0.3 μl/sec in grove and 2.0 μl/sec in pool.10 φ, which is reciprocally related to the speed of nectar extraction, is set to be in the range  $1.93 \times 10^{-5} - 3.86 \times 10^{-5}$ 10-5 (µl/day)-1. Other studies find that a bee will visit 8 -10 flowers per visit.11 Since only about 5-75 % of the flowers are perfect, the number of ovules fertilized per visit,  $k_1$ , will be in the range of 0.4 - 7.5 flowers per visit.

The normal death rate of the bees has been changing. The French National Bee Surveillance Unit  $^{12}$  has stated that the death of the bees during the winter months was one out of ten in previous years. Now, the death rate is six out of ten. This means that  $\lambda$  is in the range 0.001 - 0.006. For the birth rate of the bees,  $\delta_1$ , we assume that the queen bee lays about 1200 - 2000 eggs/day. For a typical small hive containing perhaps 20,000 bees,  $^{9,13}$  the birth rate of the bees would be in the range, 0.06-0.1 day  $^{1}$ . The estimated values of the parameters are listed in Table I.

### IVb. Numerical Solutions.

For the purpose of getting an idea of what might occur, we have set the values of the parameters at: a =500, b = 1/8,  $\lambda$  = 0.0035,  $k_1$  = 3.95,  $k_2$  = 0.00005,  $m_1$  = 7.5,  $m_2$  = 1.6,  $\phi$  = 0.0000386,  $\sigma$  = 0.25,  $\gamma$  = 0.0111,  $\mu$  = 23 and  $\delta$  = 0.05. Substituting the above values into eqns. (4a)-(4c), we get the steady state

Table 1. Parameter values

Parame	eters Units	parameter range
a	no. of flower	500
Ъ	1/(bee day)	1/8
ķΚ	no. of bee	$\frac{\delta_1 - \lambda}{b}$
ιk,	mango/(bee visit)	0.4 - 7.5
μ	microliter/visit	. 22.72-63.63
ŀφ	(microliter/day)-1	1.93x10 <sup>-5</sup> - 3.86x10 <sup>-5</sup>
.;σ	-	0.21 - 1.0
∄δ,	day- <sup>l</sup>	0.06 - 0.1
δ   δ <sub>1</sub>	day-1	0.001 - 0.006
Ϊk,	microliter <sup>-1</sup>	>1.48x10 <sup>-6</sup>
" y "	day-1	0.0111
"m	mango/day	10.93-910.75
. m,	day- <sup>1</sup>	0.63 - 2.7
δ	day-1	0.01-0.05

 $\overline{E}(0.637873, 16.129, 29.4689)$ . (35) Substituting the values of  $(\overline{x}, \overline{y}, \overline{z})$  given by eqns. (4a)-(4c) and the values of the parameters into eqn. (7), we find that the Routh-Hurwitz conditions are met and the steady state is stable. Substituting the same values in eqn. (34), we find that the critical value is

$$\tau_{o} = 1.13 \text{ days}$$
 . (36)

As τ crosses this value, the steady state should become unstable. To see if this happens, we have solved eqns. (2a), (2b') and (2c) (for a delay time of 1 day) using the values of the parameters given above. In Figure 1, we see the trajectory of the solution spiral into the equilibrium state, eqn. (35). This would be expected since  $\tau < \tau_0$ . We then changed the value of the time delay to be 1.13 days. The trajectory is now a limit cycle (See Figure 2). As we have pointed out, the conditions for the system to undergo a Hopf bifurcation to a limit cycle are met with the values of the parameters used. Finally, we pick  $\tau = 10$  days. In Figure 3, we see the trajectory spiraling away from the steady state E(0.637873, 16.129, 29.4689). The trajectory initially starts at the left face of the cube, heads towards the steady state and then spirals away from the steady stater. This implies that the steady state has become unstable.

To understand why this happens, let us look at the biology. A nonzero steady state with  $\bar{y} \neq 0$  would be possible if a new plant would begin to flower while some of the original flowers are still present. This would require that a flower, pollinated at the beginning of the flowering season, would quickly develop into a seed. The seed must then fall to the ground and germinate into a plant that develops new flowers before the original flowers dry up and die. This does not usually happen in nature. Each step in the developmental stage of the plant takes time. Since the new plants do not usually arrive until the next year, the delay time appearing in eqn. (2b') would be one year. Between the period the time the last flowers of the season die and the new ones arrive, there would be no flowering plants present.

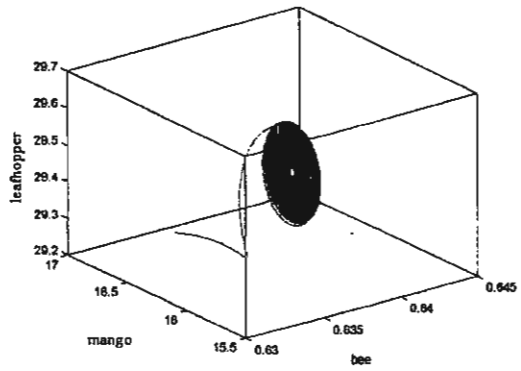


Fig 1. Numerical solution of equations (2a), (2b') and (2c) for a time delay of t=1 ( $t< t_0$ ). The graph shows the trajectory in the 3-D phase plane. The motion spirals toward the steady state solution  $\overline{R}(0.637873, 16.129, 29.4689)$ . The parameters used are: a=500, b=1/8, d<sub>1</sub>=0.08, l=0.0035, k<sub>1</sub>=3.95, k<sub>2</sub>=0.00005, m<sub>1</sub>=7.5, m<sub>2</sub>=1.6, j=0.0000386, s=0.25, g=0.0111, m=23, d=0.05

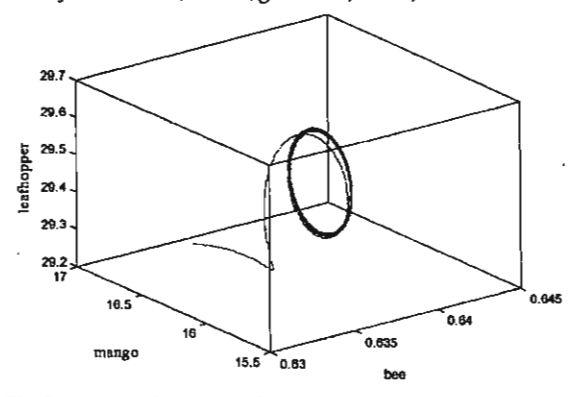


Fig 2. Numerical solution of equations (2a), (2b') and (2c) at the critical time delay t<sub>o</sub>= 1.13 days. The parameters used are: the same as used for Figures 1. The trajectory projected on 3- dimensional phase plane. The motion is a limit cycle.

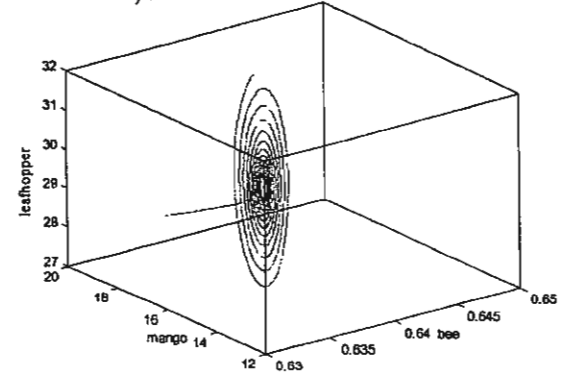


Fig 3. Numerical solution of equations (2a), (2b') and (2c) for a time delay of t=10 (1>t<sub>0</sub>) days. The graph shows the trajectory in the 3-D phase plane. The trajectory moves away from the steady state solution. The parameters used are the same as those used to obtain Figs. 1 and 2.

This would happen if the time delays are greater than the lifetime of the flower, which we have taken to be nine days.

### IVc. Real Applications.

To see how the present model might be of use to the farmers, we have modified the model to more accurately describe the production of mangos. We have inserted into eqn. (2b'), the added term  $\Phi\delta(t-t_a)$  to represent the appearance of non pollinated flowers on the tree at time t.  $\Phi$  is the number of flowers that appear on day t. We have assumed that the time delay is six months which is greater than the critical delay time. Therefore there will be no contribution from the term given by eqn. (1) in eqn. (2b'). We now look to see what would happen if the farmer has more bees on his farm. To see this, we have solved eqns. (2a), (2b') and (2c) using K values of 1000, 1,500 and 2000. The values of the other parameters are given on the figure captions. In Figure 4, we plot the number of flowers on a single tree that get pollinated each day after day to, the day the flowers began to bloom. The initial conditions for the starting day of the computer simulation, are Y(0) = 0, and X(0) and Y(0) are arbitrary. As the time passes, the number of bees begins to increase until it reaches the saturation value K. On the 100th, the flowers bloom. The figure shows that only for a short period do pollinated flowers get produced. The reason for this is that only during these nine days are the non pollinated flowers present. After this period, the flowers dried up and died. This  $\overline{lead}$  to y = 0. We also see that the number of flowers that get pollinated increases as the number of bee increases. The three plots provide a quantitative measure of how much more mangoes can be obtained by increasing the number of bees

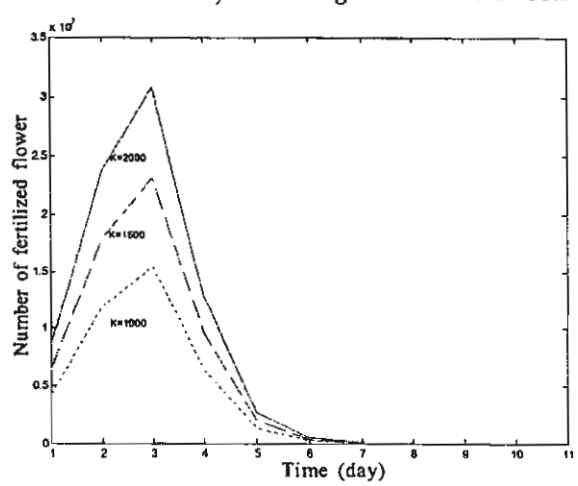


Fig 4. Number of flowers pollinated per day per tree for K equal to 1,000, 1,500 and 2,000. The number of flowers appearing on day t<sub>o</sub> is F=10,500,000. The values of the other parameters are the same as used to obtain figs. 1, 2 and 3.

available.

Another practice that can be carried out by the farmer is to decrease the number of leafhoppers. Spraying insecticides or introducing biological pests of the leafhoppers to kill them would accomplish this. The first method would however also decrease the number of bees unless the insecticide is of a type that only affects the leafhoppers and not the bees. We simulate the effects of employing an insecticide of this type or using the second method by increasing the value of the leafhopper's death rate. We have solved eqns. (2a), (2b') and (2c) for three values of the death rate  $\delta$  (0.05, 0.07 and 0.09). In Figure 5, we see that more flowers would be pollinated if the life time (inversely proportional to the death rate) of the leashopper were shorten. The time axis is changed so that it starts at day 100. We see that the flowers are only pollinated over a nine day period (i.e., during the period

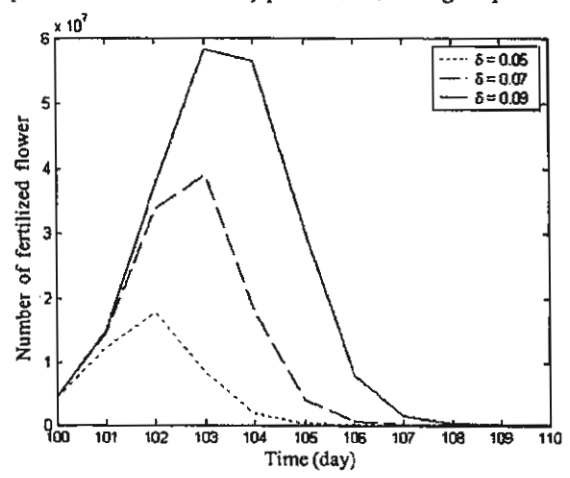


Fig 5.A graph shows the number of fertilized flower per day per tree for the death rate of leafhopper, d, equal to 0.05, 0.07 and 0.09. The number of flowers appearing on day  $t_0$  is F=10,500,000. The values of the parameters are: a=500,  $d_1$ =0.08, l=0.0035,  $k_1$ =3.95,  $k_2$ =0.00005,  $m_1$ =7.5,  $m_2$ =1.6, f=0.0000386, s=0.25, g=0.0111, m=23, b=  $d_1$ -1, K=1000

the flowers are present on the tree).

Another way for the number of pollinated flowers to be increased is to increase the number of flowers on the tree. This could be done by having the rain arrive at the right time and or having a new variety of mango plants that have more flowers. These are however beyond the control of the farmer.

### REFERENCES

- Bandyopadhyay M, Bhattacharyya R, Mukhopadhyay B, (2004). Dynamics of an autotroph-herbivore ecosytem with nutrient recycling. Ecological Modelling 176, 201-9.
- 2. Marsden JE, McCracken M, (1976). The Hopf Bifurcation and

and

and

Its Application. Springer Verlag. New York.

 Jang SR, (2002). Dynamics of herbivore-plant-pollinator models. J. Math. Biol. 44, 129-49.

- Khan QJA, Greenhalgh D, (1999), Hopf bifurcation in epidemic models with a time delay in vaccination. IMA J. Math. Appl. Med. Biol. 16, 113-42.
- Xiao Y, Chen L, (2001). Modeling and analysis of a predatorprey model with disease in the prey. Math. Bioscience 171, # 59-82.
- Tam J. (1999). Delay effect in a model for virus replication. IMA J. Math. Appl. Med. Biol. 16, 29-37.
- Jamjanya T, Siri N, Kamarsa R. The mango leafhopper. (Homoptera. Dicadellidae) October 17, 2003. Available at http://www.agserver.kku.ac.th/kaenkaset/esearch/htm/perter/16-ok.ok.htm
- Boongird S, Bees and Honey Bees. (Funny Publishing, Bangkok (2001))
- Wangnai W, The Mango (Srisombat Publishing, Bangkok (1995)).
- In Plant-Pollinators Introduction, November 13, 2003.
   Available at http://www.d.umn.edu/~teraig/doevd/doevp-ollinators.htm
- Wongsiri S. Bee-keeping in Thailand, (Funny Publishing, Bangkok (1985))
- Laurenson J, Plight of France's honey bee, October 14, 2003.
   Available at http://www.news.bbc.co.uk/1/ni/world/europe/3173400.stm
- In Question and Answers. November 1, 2003. Available at http://www.nakhonsawan.go.th/q.bee.htm

### APPENDIX

### Lemma 1. Conditions for the Existence of Positive Real Roots of a Cubic Equation.

Consider the following cubic equation

$$S(\eta) = \eta^3 + d_1 \eta^2 + d_2 \eta + d_3 = 0$$
 (A1)

**A.** If either (i)  $d_1 < 0$ ,  $d_2^3 = 0$  and  $d_1^2 > 3d_2$ , or (ii)  $d_2 < 0$ : and  $\Delta < 0$ , then eqn. (A1) has positive simple roots.

where

5

$$\Delta = S(\varepsilon_1)S(\varepsilon_2) = \frac{4}{27}d_2^3 - \frac{1}{27}d_1^2d_2^2 - \frac{2}{3}d_1d_2d_3 + \frac{4}{27}d_1^3d_3 + d_3^2$$
(A2)

with  $\varepsilon$ , and  $\varepsilon$ , being the two turning points of  $S(\eta)$  given by

$$\varepsilon_1 = \frac{-d_1 - \sqrt{d_1^2 - 3d_2}}{3}, \varepsilon_2 = \frac{-d_1 + \sqrt{d_1^2 - 3d_2}}{3}$$
 (A3)

**B.** If  $d_3 \ge 0$ , the necessary condition for eqn. (A1) to have no positive

real roots are either

(i) 
$$d_1^2 < 3d_2$$

(ii) 
$$d_1^2 = 3d_2$$

(iii) 
$$d_1^2 - 3d_2 > 0$$
 and  $\Delta > 0$ , or

(iv) 
$$d_1^2 - 3d_2 > 0$$
 and  $\Delta < 0$ ,  $d_1 > 0$  and  $d_2 > 0$ 

Proof of this lemma is found in Khan and Greenhalgh [4]. Theorem 1. (Routh-Hurwitz Criteria). Let  $x^*$  be an equilibrium point of eqn. (A4), and J be the Jacobian evaluated at the equilibrium point. Suppose the diagonalization of J yields the following characteristic equation

$$\lambda^3 + A\lambda^2 + B\lambda + C = 0 . \quad (A6)$$

The equilibrium state x\* will be local asymptotically stable if the coefficients A,B and C satisfy the following conditions:

**Theorem II. (Hopf Bifurcation).** Suppose the functions  $F_i(\{x\})$  depends on parameter  $\tau \in \mathbb{R}$ . The Jacobian will now depend on the parameter  $\tau$ , i.e.,

$$J(\tau) = D_{x}F(x^{*},\tau) = \frac{\partial F_{i}}{\partial x_{j}}(x^{*},\tau) \qquad i, \quad j = 1,2,...,n$$

If  $J(\tau)$  has a pair of complex eigenvalues,  $\lambda(\tau a) = u(\tau) \pm iv(\tau)$  such that

i. 
$$u(\tau_o) = 0$$
,  
ii.  $v(\tau_o) = v^* > 0$   
iii.  $\frac{du}{da}(\tau_o) \neq 0$  (A8)

where  $\tau_a$  is called a critical value of the bifurcation parameter ' $\tau$ ', and no other eigenvalues with zero real part exist, the system will undergo a transition to a limit cycle about the point ( $\mathbf{x}^*$ ,  $\tau_a$ ).

Proofs of this theorem can be found in various textbooks.<sup>2</sup>

JOURNAL OF BIOSCIENCE AND BIOENGINEERING Vol. 98, No. 3, 182–186, 2004

\*\*\*

1

ri

ıİ

# Effects of Static Magnetic Field on Growth of Leptospire, Leptospira interrogans serovar canicola: Immunoreactivity and Cell Division

WANNAPONG TRIAMPO, 1.4\* GALAYANEE DOUNGCHAWEE, 2 DARAPOND TRIAMPO, 3 JIRASAK WONG-EKKABUT, 1 AND I-MING TANG 1.4

Department of Physics, Faculty of Science, Mahidol University, Bangkok 10400, Thailand, Department of Pathobiology, Faculty of Science, Mahidol University, Bangkok 10400, Thailand, Department of Chemistry, Faculty of Science, Mahidol University, Bangkok 10400, Thailand, and Capability Building Unit in Nanoscience and Nanotechnology, Faculty of Science, Mahidol University, Bangkok 10400, Thailand

Received 4 March 2004/Accepted 14 June 2004

The effects of the exposure of the bacterium, Leptospira interrogans serovar canicola to a constant magnetic field with magnetic flux density from a permanent ferrite magnet=140±5 mT were studied. Changes in Leptospira cells after their exposure to the field were determined on the basis of changes in their growth behavior and agglutination immunoreactivity with a homologous antiserum using dark-field microscopy together with visual imaging. The data showed that the exposed Leptospira cells have lower densities and lower agglutination immunoreactivity than the unexposed control group. Interestingly, some of the exposed Leptospira cells showed abnormal morphologies such as large lengths. We discussed some of the possible reasons for these observations.

[Key words: leptospirosis, Leptospira interrogans, magnetic field, dark-field microscopy, immunoreactivity, cell division]

Leptospirosis is an acute febrile illness caused by pathogenic spirochete bacteria of the genus Leptospira (1, 2). This disease has emerged as an important public health problem worldwide. The symptoms of this disease can range from mild-flu-like symptoms to severe (often fatal) complications such as renal and/or liver failure and hemorrhage (referred to as Weil's syndrome) (3). Most outbreaks tend to be seasonal in nature and are often associated with environmental factors, animals, and agricultural and occupational cycles such as rice cultivation in marshy lands. Mammals such as rats and cattle are commonly involved in the transmission of this disease to humans via direct or indirect exposure to contaminated tissues or urine (1, 2, 4). Out-breaks of leptospirosis occur mainly after flood, making it an occupational hazard for sanitary and agricultural workers, as well as a recreational hazard for humans (5). Some pathogenic Leptospira species have also been found to be associated with domesticated animals. For example, serovar canicola (Leptospira canicola) has adapted itself to canines; therefore, it has become common in many human communities. Although there has been no report of leptospirosis in canines in Thailand, there is a great potential for the transmission of the disease between humans and dogs kept as household pets, unless one is aware of the disease.

\* Corresponding author. e-mail: scwtr@mahidol.ac.th; wtriampo@yahoo.com phone: +66-2-889-2337 fax: +66-2-354-7159

L. canicola cells used in our study are motile aerobes that are very thin, flexible and spiral-shaped of about 0.1 µm width and 6-20 μm length. Leptospira cells are difficult to observe under a light microscope. They can, however, be observed by dark-field microscopy using wet samples. This allows for the determination of agglutination immunoreactivity to be determined. The Leptospira outer membrane or surface antigens can be detected through its agglutination with a homologous (antiserum). The optimal conditions for its growth and as well, its biology are well documented in the literature (1, 2). Moist environments with a neutral pH are suitable conditions for the survival of Leptospira outside the host. The optimal cultivation temperature is approximately 20-32°C. In general, Leptospira species are highly susceptible to adverse environmental conditions such as exposure to dry air, chemicals such as chlorine or iodine in detergents, unfavorable pH (>8.0 or <6.5), strong electromagnetic fields and high temperatures (above 40°C).

Magnetic fields (MFs) also affect various biological functions of living organisms, for example, DNA synthesis and transcription (6), as well as ion transportation through cell membranes (7). Almost all living organisms are exposed to magnetic fields from various sources. The geomagnetic field on the surface of the earth is approximately 0.50–0.75 gauss in strength. There have been several studies on the effects of exposure to MFs and several of these have given rise to controversies over the past decades. The growth rate of the Burgundy wine yeast has been shown to decrease when an ex-

tremely low magnetic flux density (MFD) of 4 gauss is applied (8). The growth of *Trichomonas vaginalis* is accelerated when it is exposed to 460–1200 gauss (9). The growth rate of *Bacillus subtilis* increases when exposed to 150 gauss and decreases when exposed to more than 300 gauss (10). Similar results were reported for *Chlorella*; an exposure of less than 400 gauss increases the growth, while exposure to 580 gauss decreases the growth rate (11). Several studies point to the MF as a factor influencing the growth and survival of living organisms, which vary at different MFDs (12–15). Other researchers have studied the effects of MFs on bacteria at the enzyme (16) or genetic (17) level.

To study the efficacy of using magnetic field to control or prevent the growth of leptospire, we applied MF on selected *Leptospira* cells at various intensities and exposure duration levels. We then determined the agglutinating activity of experimental bacteria using dark field microscopy.

### **MATERIALS AND METHODS**

Pathogenic Leptospira interrogans, serovar canicola was used in this study. Bacterial cells were grown in the Ellinghausen and McCullough modified by Johnson and Harris (EMJH) liquid medium (2). The bacterial cells were grown at a temperature of  $27\pm1^{\circ}\text{C}$  in the dark.

A cylindrical permanent ferrite magnet 5 cm in diameter was placed beside 15 ml culture glass tube (less than 1 ml apart) containing 1 ml of a suspension of newly subcultured Leptospira cells in the EMJH liquid medium. MF and homogeneity of 140±5 mT (northpole) were checked using a teslameter (Hall effect Teslameter digital, order no. 13610.93; Phywe Systeme, Göttingen, Germany). The intensity of static magnetic field used in our experiments was chosen on the basis of Genkov et al. (9) findings. Genkov et al. had used more or less this intensity of a constant MF to induce the growth and development of Trichomanas vaginalis. For this type of exposure, no shielding against the natural variations of terrestrial MF was required, the value of approximately 0.050 mT is negligible with respect to the MF intensities applied. An experiment using cells not exposed to MF was simultaneously performed as the control, which was placed at a distance of about 100 cm from the exposed group.

In the absence of magnets, MFD was 0.05±0.01 mT. All bacterial samples were exposed to MF for different durations, that is, 0 (control sample), 1, 2, 3, 4, 5, and 6 d. After MF exposure, individual samples were further incubated for 7 d. Immediately after 7 d of incubation, dark-field micrographs were taken using a CCD camera to observe cell development. The growth and agglutination properties using the microscopy agglutination test (MAT) with a homologous antiserum and immunoreactivity were scored as follows:

- 4+ = 100% absence of Leptospira cells from the field
- 3+=75% absence of *Leptospira* cells from the field
- 2+=50% absence of *Leptospira* cells from the field
- 1+ = 25% absence of Leptospira cells from the field

MAT has been commonly used as a diagnostic tool for leptospirosis. This may not be the most reliable test. It, however, is arguably the most appropriate test for this study. The same set of conditions and specimens were used in the experiments, which were repeated twice.

Atomic force microscopy (AFM) and sample preparation Scanning probe microscopy (SPM) (Digital Instruments Veeco Metrology Group, NY, USA) was used for AFM surface morphol-

Metrology Group, NY, USA) was used for AFM surface morphology imaging. Images were acquired in the contact mode showing height contours that highlight the spiral shape and fine surface

morphology of *Leptospira* cells. An AFM scanner with hardware correction for the nonlinearities of the piezoelectric element was used. The scanner has a maximum xy range of 125 by 125  $\mu m$  and a Z range of 6  $\mu m$ . The cantilevers of  $Si_3N_4$ , 125  $\mu m$  long and 35  $\mu m$  wide with a spring constant of 0.58 Nm $^{-1}$  were used. To locate the area of interest in the samples and identify any bacteria, we used a built-in long-range on-axis microscope, capable of a 5:1 zoom and  $\times 3500$  magnification. Imaging was carried out at scan speeds between 1 and 50  $\mu m/s$ . Images were acquired at 256  $\times 256$  pixels. A typical imaging session began using a built-in optical microscope and by moving the x-y table to search for bacterial cells. The AFM cantilever was then moved forward to the surface close to the chosen bacterial cell.

Each sample was prepared using the method described above. It was then dropped on a microscope glass slide and dried in air.

### RESULTS

Figure 1 shows the AFM picture of an *L. interrogans* serovar *canicola* cell taken with a Digital Instrument Nanoscope IIIa (Digital Instruments Veeco Metrology Group) in the contact mode. The image shows a normal morphology of *L. interrogans* serovar *canicola*, that is, the spiral shape. It is worth noting that AFM usually reveals the actual roughness of the surface of the bacterial envelope. Other types of microscopy frequently show the surface to be relatively smooth. This technique was also used to observe the surface morphology of bacterial cells before and after the exposure to MF. It should be noted that this image does not demonstrate the rough envelope very clearly. However, it does show the normal bacterial morphology.

Figure 2 shows some representative dark field micrographs of *L. interrogans* serovar *canicola* taken at the logarithmic growth phase (at 1:10 dilution of culture samples) and for different durations of MF exposure, that is, 0, 2, 3, and 6 d. After 7 d of incubation, the samples were observed

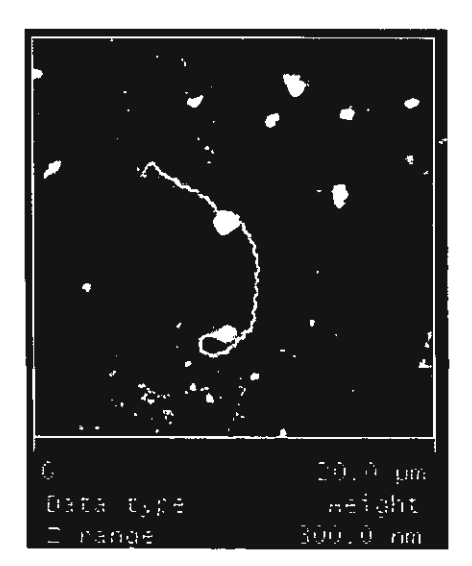


FIG. 1. Atomic force micrograph (AFM) of Leptospira interogans serovar canicola taken using Digital Instrument NanoScope IIIa in the contact mode under control conditions, that is, without MF exposure. Scan size was 20  $\mu m$  and scan rate was 1 Hz. It shows a spiral-shaped leptospire of approximately  $10{-}20~\mu m$ .

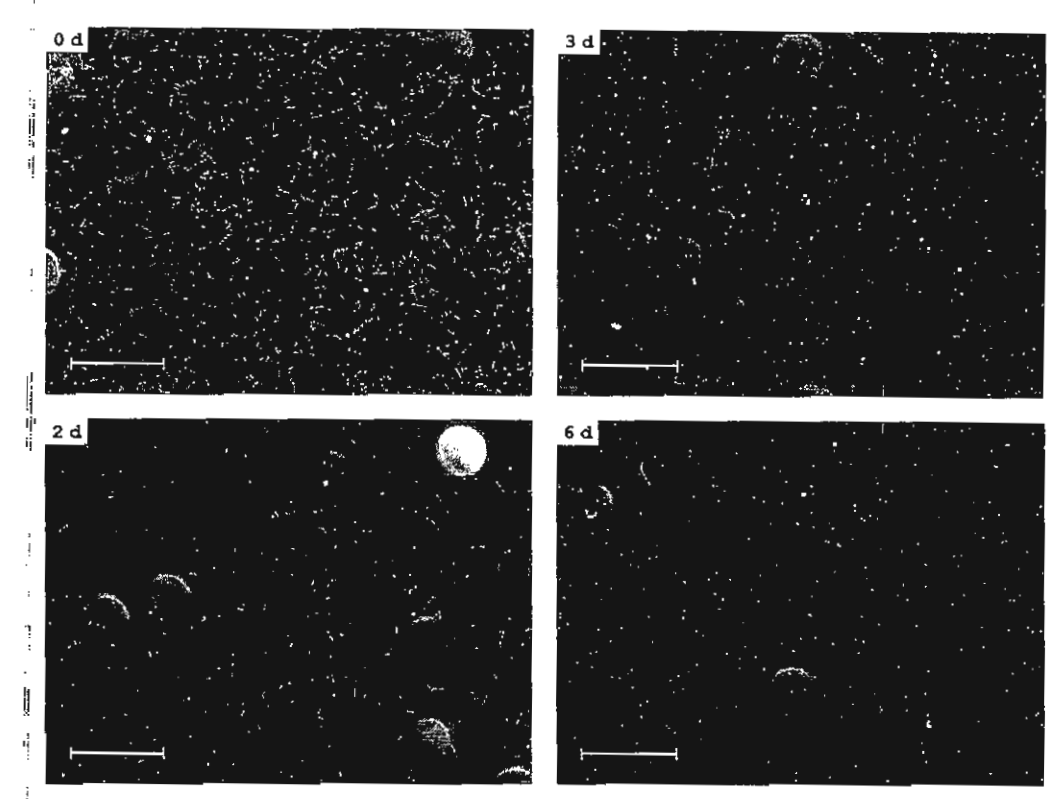


FIG. 2. Dark field micrographs of *L. interrogans* serovar canicola exposed to MF for different durations. The images were taken at the log phase of each experimental culture sample (diluted 1:10 of original). Bars: 100 μm.

under a dark field microscope and images were taken using a CCD camera. Even though there are some noises in the images, the inhibition of cell growth could be observed. The implications of these observations are significant given the results of other studies (6–17). From Fig. 2A to 2D, one can clearly observe that cell density decreased with exposure time, particularly after more than 3 d. This indicates the decrease in growth rate resulting in the decrease in the number of bacterial cells. This is one of the factors that explain the lower agglutination immunoreactivity, which indicates fewer

remaining living bacterial cells to agglutinate.

Figure 3 shows the dark field micrographs of agglutinated bacterial cells after reacting with the specific antiserum; Fig. 3A shows a complete agglutination (100% immuno) and Fig. 3B shows 50% agglutination (with only one half of free-living bacterial cells present).

On the basis of the criteria mentioned at the end of the previous section, the agglutination reactivities of the *L. interrogans* serovar *canicola* exposed to different intensities of MF are listed in Table 1 (with longer exposure time, the

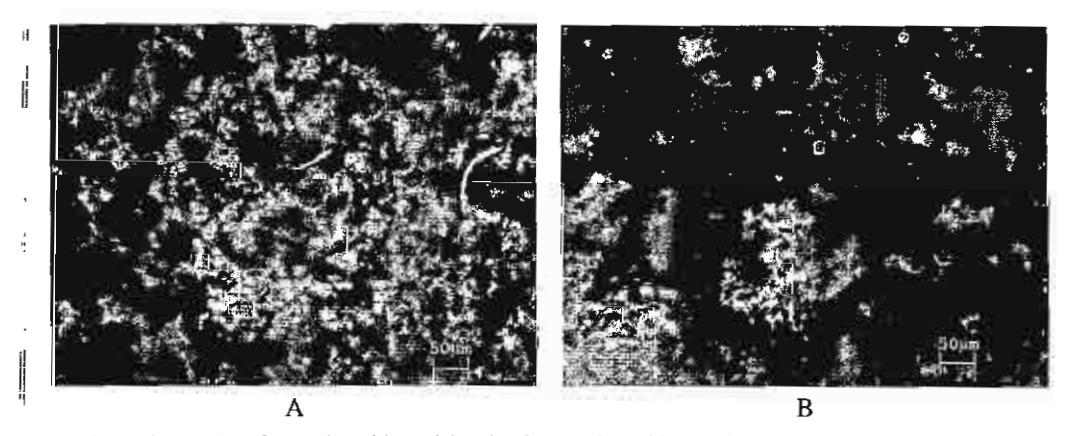


FIG. 3. Dark field micrographs of agglutinated bacterial cells after reacting with homologous antiserum, showing complete agglutination (100% reactivity; A) and 50% agglutination with one-half of free-living bacterial cells remaining (B).

TABLE 1. Agglutination characteristics of leptospires after magnetic field exposure for various durations

Exposure duration (d)	l : 50 dilution	1:100 dilution	1:200 dilution	1:400 dilution	1:800 dilution	1:1600 dilution	1:3200 dilution
Oa	4+	3+	2+	2+	2+	2+	1+
1	3+	2+	<b>i</b> +	-	_	_	_
2	3+	2+	1+	_	_	_	_
3	2+		_	_	_	_	_
4	2+	_	_	_	_	_	_
5	1+		_	_	_	_	_
6	NA	_	-	_	_	_	_

<sup>&</sup>lt;sup>a</sup> Representive sample of control unexposed leptospires showing a higher MAT titer (1:1600) than exposed samples for various durations. NA indicates no agglutination occurred.

#### Agglutination immunoreactivity

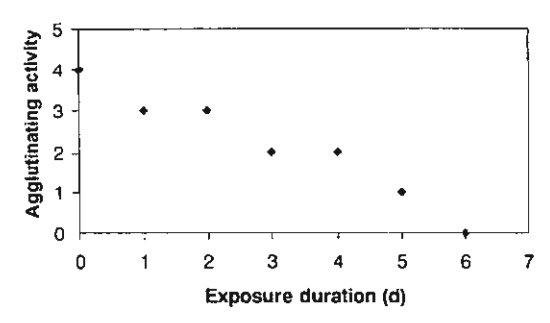


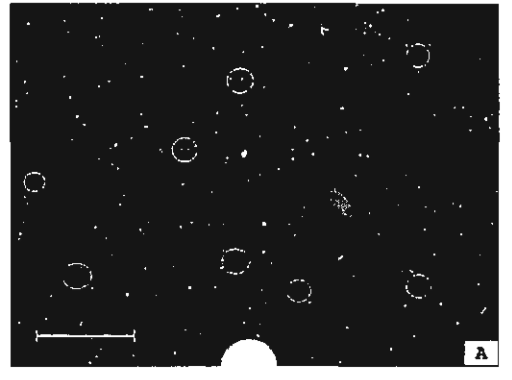
FIG. 4. Plots of data shown in Table 1.

Leptospira bacterial cells demonstrated a lower agglutination immunoreactivity than that of the reference antiserum tested. The end point of reactivity was 50% agglutination [2+]). The agglutination immunoreactivity score decreased with exposure time of Leptospira cells as shown in Fig. 4. Comparing the MAT results of control Leptospira cells (0 d exposure) and those of bacterial cells after exposed to MF, we found that the latter groups (particularly those with longer exposure) showed lower agglutination reactivies. These findings may indicate the presence of a lower amount of agglutinin or number (density) of Leptospira cells in the exposed samples than in the control samples. It should be emphasized that the same set of conditions and specimens were

used in the experiments that were repeated twice, and the experiments yields exactly the same (semiquantitative) results. The scoring data therefore did not show an error. Once again, in each experimental setup, it has one control (non-exposed) group and six exposed groups with different durations of exposure.

Besides the decrease in the number of Leptospira cells as the cause of the decrease in agglutination immunoreactivity as mentioned above, the "denaturing effect" of the antigenantibody reaction may be an other contributing factor to this phenomenon, which can be explained as follows: Typically, antibodies are large soluble protein molecules known as immunoglobins and are produced by B-cells. They bind to specific antigens in a lock-and-key fashion (lock = antibody; key = antigen) (18). Their shape should, therefore, be specific to particular antigens. When a specific antibody encounters an antigen, it will form an antigen-antibody complex through some noncovalent forces such as electrostatic force, hydrogen bond, van der Waal force or hydrophobic force. When a change in what of a single atom occurs, the complex can become unbound. This specificity could be the underlying factor for the denaturation of the antigen-antibody reaction. Under the conditions used in the study, the motion or transfer of any electrons or ions onto the cell membrane could induce an electric current. This current may perturb the other charge particle motion in the cell thus resulting in the loss of binding (19).

Surprisingly, we observed that some Leptospira cells exposed for three or more days were longer than the control



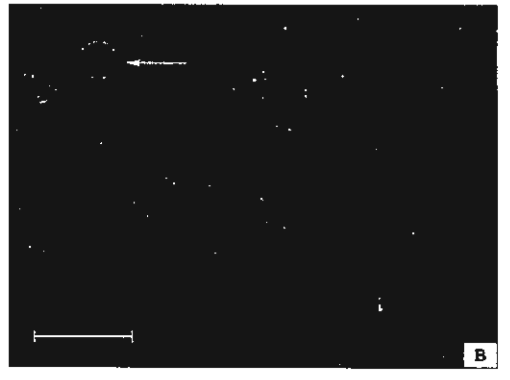


FIG. 5. Dark-field micrographs of *L. interrogans* serovar *canicola* taken at the same magnification ( $\times$ 200). Control sample unexposed to magnetic field; the leptospires have an approximate length of  $10-20~\mu m$  (A) compared with magnetic field-exposed leptospires (B) with some cells longer than others. Circles indicate individual bacterial cells. Bars:  $100~\mu m$ .

TRIAMPO ET AL.

J. BIOSCI, BIOENG.

bacterial cells (see Fig. 5). This preliminary finding probably indicates that there is some disturbance in cell division. More experiments must be carried out to examine and determine the exact mechanism underlying these observed phenomena. Our present explanation for this abnormality in cell division is based on the following: Like most bacteria and archaea, Leptospira cells divide symmetrically possibly via the formation of a septum in the middle of the cell (we consider that binary fission is less likely). For the time being, we use AFM in the investigation of division-related morphologies. Recent evidence indicates that synthesized proteins dedicated to cell division are assembled between segregated chromosomes at an appropriate time (20). The key to this assembly is the filamentous temperature exposure sensitive (Ftsz structural) analogue of tubulin (21). DNA damage caused by MF exposure induces mutation, resulting in the abnormal synthesis of FtsZ, which in turn could interfere or stop cell division. Similar to previous studies of Escherichia coli, FtsZ appears to induce the earliest (known) step in cell division. E. coli cells with a mutation of ftsz caused by exposure to certain conditions do not divide. This result in the formation of long filamentous cells that can replicate and segregate their chromosomes (22).

Our finding is at least the first step toward a grater understanding of the development of diagnostics, treatment, and prevention schemes for bacterium and leptospirosis. We hope that further studies of leptospirosis will lead to this disease in the near future.

### ACKNOWLEDGMENTS

This research was supported in part by the Thailand Research Fund, TRG4580090 and RTA4580005 and MTEC Young Research Group funding MT-NS-45-POL-14-06-G. The support of the Royal Golden Jubilee Ph.D. Program (PHD/0240/2545) to Jirasak Wong-Ekkabut and I-Ming Tang is also acknowledged.

### REFERENCES

- 1. Faine, S. (ed.): Guideline for control of leptospirosis, vol. 67,
- p. 129. World Health Organization, Geneva (1982).
  Faine, S., Adler, B., Bolin, C., and Perolat, P.: Leptospira and Leptospirosis, 2nd ed., p. 272. MediSci Ed, Melbourne
- 3. Sherris, J. C.: An introduction to infectious disease, 2nd ed., o. 432-435. Elsevier, New York (1990).
- Turner, L. H.: Leptospirosis I. Trans. R. Soc. Trop. Med. Hyg., 61, 842-855 (1967).
- 5. Benenson, A.S.: Leptospirosis, p. 293-296. In Chin, J. E. (ed.). Control of communicable diseases manual, American

- Public Health Association, Washington, D.C. (2000).
- Phillips, J. L., Haggren, W., Thomas, W. J., Ishida-Jones, T., and Adey, W. R.: Magnetic field-induced changes in specific gene transcription. Biochim. Biophys. Acta, 112, 140-144 (1992)
- 7. Liburdy, R. P., Callahan, D. E., Harland, J., Dunham, E., Sloma, T. R., and Yaswen, P.: Experimental evidence for 60 Hz magnetic fields operating through the signal transduction cascade: effects on calcium influx and c-MYC mRNA induction. FEBS Lett., 334, 301-308 (1993).
- Kimball, G. K.: The growth of yeast in a magnetic field. J. Bacteriol., 35, 109-122 (1938).
- Genkov, D., Cvetkova, A., and Atmadzov, P.: The effect of the constant magnetic field upon the growth and development of T. vaginallis. Folia Medica, 16, 95-99 (1974).
- 10. Moore, R. L.: Biological effects of magnetic fields: studies with microorganisms. Can. J. Microbiol., 25, 1145-1151 (1979)
- Takahashi, F. and Kamezaki, T.: Effect of magnetism of growth of Chlorella. Hakkokogaku, 63, 71-74 (1985)
- Yamaoka, Y., Takimura, O., Fuse, H., and Kamimura, K.: Effect of magnetism on growth of *Dunaliella salina*. Res. Photosynth., 3, 87-90 (1992).

  13. Singh, S. S., Tiwari, S. P., Abraham, J., Rai, S., and Rai,
- A. K.: Magnetobiological effects on a cyanobacterium, Anabena
- doliolum. Electro- Magnetobiol., 13, 227-235 (1994).

  Tsuchiya, K., Nakamura, K., Okuno, K., Ano, T., and Shoda, M.: Effect of homogeneous and inhomogeneous high magnetic fields on the growth of Escherichia coli. J. Ferment. Bioeng., 81, 343-346 (1996).
- Piatti, E., Albertini, M. C., Baffone, W., Fraternale, D., Citterio, B., Piacentini, M. P., Dacha, M., Vetrano, F., and Accorsi, A.: Antibacterial effect of a magnetic field on Serratia marcescens and related virulence to Hordeum vulgare and Rubus fruticosus callus cells. Comp. Biochem. Physiol. B. Biochem. Mol. Biol., 132, 359-365 (2002).
- Utsunomiya, T., Yamane, Y., Watanabe, M., and Sasaki, K.: Stimulation of porphyrin production by application of an external magnetic field to a photosynthetic bacteria, Rhodo-
- bacter sphaeroides. J. Biosci. Bioeng., 95, 401-404 (2003). Horiuchi, S., Ishizaki, Y., Okuno, K., Ano, T., and Shoda, M.: Drastic high magnetic field effect on suppression of Escherichia coli death. Bioelectrochemistry, 53, 149-153 (2001)
- Boyd, R. F.: Basic medical microbiology, 5th ed. Little, Brown and Co., Boston (1995).
- Jackson, J. D.: Classical electrodynamics, 3rd ed. Wiley Text Books, New York (1998).
- Rothfield, L., Justice, S., and Garcia-Lara, J.: Bacteria cell division. Annu. Rev. Genet., 33, 423-448 (1999).
- Lutkenhaus, J.: Ftsz ring in bacterial cytokinesis. Mol. Microbiol., 9, 403-410 (1993).
- Hale, C. A. and de Boer, P. A. J.: Direct binding of FtsZ to ZipA, an essential component of the septal ring structure that mediates cell division in E. coli. Cell, 88, 175-185 (1997).

Journal of the Korean Physical Society, Vol. 46, No. 4, April 2005, pp. 0~0

П

Ľ,

į.

||-

# A Lattice Boltzmann Method for Modeling the Dynamic Pole-to-Pole Oscillations of Min Proteins for Determining the Position of the Midcell Division Plane

Waipot NGAMSAAD, Wannapong TRIAMPO,\* Paisan KANTHANG,
I-Ming TANG, Narin NUTTAWUT and Charin MODJUNG

Department of Physics and Capability Building Unit in Nanoscience and Nanotechnology,
Faculty of Science, Mahidol University, Bangkok 10400, Thailand

Yongwimon LENBURY

Department of Mathematics, Faculty of Science, Mahidol University, Bangkok 10400, Thailand

(Received 14 September 2004)

Determining the middle of the bacteria cell and the proper placement of the septum is essential to the division of the bacterial cell. In E. coli, this process depends on the proteins MinC, MinD, and MinE. Here, the lattice Boltzmann method (LBM) is used to study the dynamics of the oscillations of the min proteins from pole to pole. This determines the midcell division plane at the cellular level. The LBM is applied to the set of deterministic reaction diffusion equations proposed by Howard et al. to describe the dynamics of the Min proteins. The LBM results are in good agreement with those of Howard et al. and agree qualitatively with the experimental results. Our good results indicate that the LBM can be an alternative computational tool for simulating problems dealing with complex biological systems that can be described by using the reaction-diffusion equations

PACS numbers: 87.15.Aa

Keywords: Lattice Boltzmann method, Bacteria, E.coli, Cell division, Min proteins, MinCDE oscillation

### I. INTRODUCTION

Cell division or cytokinesis is the process by which a cell separates into two after its DNA has been duplicated and distributed into the two regions that will become the future daughter cells. For a successful cell division to take place, the cell has to determine the optimal location of the cell separation and the time to start the cell cleavage. This involves the identification of the midpoint of the cell where the septum or cleavage furrow will form. For Escherichia coli and other rod-like bacteria, evidence accumulated over the past few years indicate that the separation into two daughter cells is achieved by forming a septum perpendicular to their long axes. To induce the separation, the FtsZ ring (Z ring), a tubulin-like GT-Pase, is believed to initiate and guide the septa growth by contraction [1]. The Z ring is usually positioned close to the center, but it can also form in the vicinity of the cell poles. Two processes are known to regulate the placement of the division site: nucleoid occlusion [2] and the action of the min proteins [3]. Both processes interfere with the formation of the Z ring, which is believed to

determine the division site. Nucleoid occlusion is based on cytological evidence that indicates that the Z ring assembles preferentially on those portions of the membrane that do not directly surround the dense nucleoid mass [4].

The min proteins that control the placement of the division site are the MinC, MinD, and MinE proteins [3]. Experiments involving the use of modified proteins show that MinC is able to inhibit the formation of the FtsZ-ring [5]. MinD is an ATPase that is connected peripherally with the cytoplasmic membrane. It can bind to MinC and activate the function of MinC [6,7]. Recent studies show that MinD recruits MinC to the membrane. This suggests that MinD stimulates MinC by concentrating it near its presumed site of activation [8, 9]. That MinE is required to give site specificity to the division inhibitor suggests that MinE acts as a topological specificity protein, capable of recognizing the midcell site and preventing the MinC division inhibitor from acting at that site [10]. Its expression results in a sitespecific suppression of the MinC/MinD action so that the FtsZ assembly is allowed at the middle of the cell, but is blocked at other sites [3]. In the absence of MinE, the MinC/MinD is distributed homogeneously over the entire membrane. This results in a complete blockage

<sup>\*</sup>E-mail: wtriampo@yahoo.com; Fax: 662-201-5843

of the Z-ring formation and the subsequent formation of a long filamentous cell which that will fail to divide 18, 9,11,12]. By fluorescent labeling, MinE was shown to attach to the cell wall only in the presence of MinD [13, 14]. Because MinD interacts with MinC, it is likely that they oscillate together. This results in a concentration of the division inhibitor at the membrane on either cell end, alternating between being high or low every other 20 seconds, so that the period of oscillation is about 40 seconds per cycle [8,9]. MinE is not only required for the MinC/MinD oscillation, it is also involved in setting the frequency of the oscillation cycle [11]. Several lines of evidence indicate that the MinE localization cycle is tightly coupled to the oscillation cycle of MinD. Recently, microscopy of fluorescently labeled proteins involved in the regulation of E.coli division uncovered coherent and stable spatial and temporal oscillations of these three proteins [15]. The proteins oscillate from one end of the bacterium to the other and move between the cytoplasmic membrane and the cytoplasm. The detailed mechanism by which these proteins determine the correct position of the division plane is currently unknown, but the observed pole-to-pole oscillations of the corresponding distribution are thought to be of functional importance.

### II. LATTICE BOLTZMANN METHOD AND MODEL DESCRIPTION

The Lattice Boltzmann method (LBM) is a numerical scheme evolved from the lattice gas model (LGM) in order to overcome the difficulties encountered with that model [16, 17]. The LGM or lattice gas automata is a method to determine the kinetics of particles by utilizing a discrete lattice and discrete time. It has provided insights into the underlying microscopic dynamics of the physical system whereas most other approaches focus only on the solution to the macroscopic equation. However, the LGM, in which the particles obey an exclusion principle, has microscopic collision rules. These rules are very complicated and require many random numbers. These random numbers create noise or fluctuations. An ensemble averaging is then required to smooth out the noise in order to obtain the macroscopic dynamics which are the results of the collective behavior of the many microscopic particles in the system and which are not sensitive to the underlying details at the microscopic level. The averaging requires a long time, which leads to an increase in the amount of computational storage required and which in turn leads to a reduction in the computational speed. For these reasons, the LBM is used only when one is interested in the evolution of averaged quantities and not in the influence of the fluctuations. The LBM gives a correct average description on the macroscopic level of a fluid. The LBM can also be viewed as a special finite difference scheme for the kinetic equation of the discrete-velocity distribution function. The simplicity and the kinetic nature of the LBM are among its appealing features.

The LBM consists of simple arithmetic calculations and is, therefore, easy to program. In the LBM, the space is divided into a regular Cartesian lattice grid as a consequence of the symmetry of the discrete velocity set. Each lattice point has an assigned set of velocity vectors with specified magnitudes and directions connecting the lattice point to its neighboring lattice points. The total velocity and particle density are defined by specifying the number of particles associated with each of the velocity vectors. The microscopic particle distribution function, which is the only unknown, evolves at each time step through a two-step procedure: convection and collision. The first step, convection (or streaming), simply advances the particles from one lattice site to another lattice site along the directions of motion according to their velocities. This feature is borrowed from kinetic theory. The second step or collision is models various interactions among particles by allowing for the relaxation of a distribution towards an equilibrium distribution through a linear relaxation parameter. The averaging process uses information based on the whole velocity phase space.

Most research reported in the literature is limited to the LBM for the Navier-Stokes equations [18,19]. The LBM scheme has been particularly successful in simulating fluid-flow applications for a broad variety of complex physical systems and has found application in different areas, such as hydrodynamic systems [17,20], multiphase and multi-component fluids [21], advection-dispersion [22] and blood flow [23–25]. Application to complex biological systems at the cellular and the molecular biological levels has been rare.

In the present paper, we propose a LBM to study the partitioning of the bacterial cell during cell division. This provides an alternative method to investigate quantitatively the division of the cell. We compare our results with those obtained by numerically solving a set of deterministic coarse-grained coupled reaction-diffusion equations [26] to demonstrate the validity of the proposed LBM.

### 1. Reaction-diffusion Equation Model

We focus on the  $E.\ coli$  bacteria, a commonly studied rod shaped bacteria of approximately  $2-6\ \mu m$  in length and around  $1-1.5\ \mu m$  in diameter. Each  $E.\ coli$  bacteria divides roughly every hour via cytokinesis. We adopted the dynamic model of the compartmentization in the bacterial cell division process proposed by Howard  $et\ al.$  In the Howard model, dynamics at the mean-field level are given by a set of coarse-grained non-linear reaction-diffusion equations. The reaction-diffusion equations to model self-organization and pattern formation [27].

Our starting point is the set of one-dimensional deterministic coupled reaction-diffusion equations used to describe the dynamics of the interactions between the local densities of MinD and MinE proteins given by Howard et al [26]. They describe the time rates of change of the densities due to the diffusions of MinD and MinE and to the mass transfer between the cell membrane and the cytoplasm. Based on the experimental results given in Ref. 9, which showed that the MinC dynamics are similar to those of MinD, we have not written out the equations for MinC. In dimensionless form, the dynamics are written as in the start of 
$$\frac{\partial n_D}{\partial t} - D_D \frac{\partial^2 n_D}{\partial x^2} = R_D = -\frac{\sigma_1 n_D}{1 + \sigma_1' n_e} + \sigma_2 n_e n_d \quad (1)$$

$$\frac{\partial n_d}{\partial t} = D_d \frac{\partial^2 n_d}{\partial x^2} = -R_D = \frac{\sigma_1 n_D}{1 + \sigma_1' n_e} - \sigma_2 n_e n_d \qquad (2)$$

$$\frac{\partial n_E}{\partial t} - D_E \frac{\partial^2 n_E}{\partial x^2} = R_E = \frac{\sigma_4 n_e}{1 + \sigma_4' n_D} - \sigma_3 n_D n_E \quad (3)$$

$$\frac{\partial n_c}{\partial t} - D_e \frac{\partial^2 n_c}{\partial x^2} = -R_E = -\frac{\sigma_4 n_e}{1 + \sigma_4' n_D} + \sigma_3 n_D n_E \tag{4}$$

where  $n_s$  is the mass density of particle of species  $s = \{D, d, E, e\}$  at time t and position x. The first equation is for the cytoplasmic MinD density  $n_D$ . The second is for the membrane-bound MinD density  $n_d$ . The third is for the cytoplasmic MinE density  $n_E$ , and the last is for the membrane-bound MinE density  $n_e$ .  $R_s$  is the reaction term and depends on the density of the species  $n_s$  and on the densities of the other species that react with species  $s.D_s$  is the diffusion coefficient. In this paper, we assume that  $D_s$  is isotropic and independent of x. The constant  $\sigma_1$  represents the association of MinD to the membrane [12].  $\sigma_1$  corresponds to the membranebound MinE suppressing the recruitment of MinD from the cytoplasm.  $\sigma_2$  reflects the rate that MinE on the membrane drives the MinD on the membrane into the cytoplasm. Based on the evidence of the cytoplasmic interaction between MinD and MinE [7], we let  $\sigma_3$  be the rate that cytoplasmic MinD recruits cytoplasmic MinE for the membrane while  $\sigma_4$  corresponds to the rate of dissociation of MinE from the membrane to the cytoplasm. Finally,  $\sigma_4$  corresponds to the cytoplasmic MinD suppressing the release of the membrane-bound MinE. The time scale of the diffusion on the membrane is much slower than that in cytoplasm. It seems, therefore, reasonable to set  $D_d$  and  $D_e$  to zero. In this dynamics, we allow for the Min protein to bind/unbind from the membrane, but not for it to be degraded in the process. Thus, the total amount of each type of Min protein is conserved. The zero-flux boundary condition will be imposed. This boundary condition gives a closed system with reflecting or hard-wall boundary conditions.

### 2. Lattice Boltzmann Equation

The dynamics determined by Eqs. (1)-(4) can be simulated using a Lattice-Boltzmann method having three one-dimensional velocities. Let  $f_s(\vec{x},i,t)$  be the one-particle distribution function of species s with velocity  $\vec{e_i}$  at some dimensionless time t and dimensionless position  $\vec{x}$ . The coordinate  $\vec{x}$  only takes on a discrete value: the nodes of the chosen lattice. The nearest neighbor vectors are defined as

$$\vec{e_i} = \begin{cases} \vec{0} & i = 0\\ \hat{x} & i = 1\\ -\hat{x} & i = 2 \end{cases}$$
 (5)

where  $\hat{x}$  is a unit vector along the x direction. For each lattice site, we have three states for each species. Following Ref. 28, the lattice Boltzmann equation for  $f_s(\vec{x}, i, t)$  can be written as

$$f_s(\vec{x} + \vec{e_i}, i, t + 1) - f_s(\vec{x}, i, t) = \Omega_s(\vec{x}, i, t)$$
 (6)

where  $\Omega_s$  is the collision operator for the species s and depends on the distribution function  $f_s$ . The collision operator  $\Omega_s$  can be separated into two parts [29], a non-reactive term  $(\Omega_s^{NR})$  and a reactive term  $(\Omega_s^R)$ , i.e.,

$$\Omega_{\varepsilon} = \Omega_{\varepsilon}^{NR} + \Omega_{\varepsilon}^{R} \tag{7}$$

In order to relate the results obtained by solving Eq. (6) with the solutions of Eqs. (1)-(4), we need to derive the evolution equations for the moments of the function  $f_s$ . The zeroth moment of  $f_s$ , the total number of particles of species s at time t and position x, is defined as

$$n_s(\vec{x}, t) \equiv \sum_i f_s(\vec{x}, i, t) = \sum_i f_s^{eq}(\vec{x}, i, t)$$
 (8)

For the nonreactive term,  $\Omega_s^{NR}$  we use the Bhatnagar-Gross-Krook (BGK) approximation with a single relaxation time  $\tau_s$  [30]:

$$\Omega_s^{NR} = -\frac{1}{\tau} [f_s(\vec{x}, i, t) - f_s^{eq}(\vec{x}, i, t)]$$
 (9)

where the equilibrium distribution function of the species  $f_s^{eq}(\vec{x},i,t)$  depends on  $\vec{x}$  and t through the local density and velocity. Here, we use the simple equilibrium distribution function corresponding to a system with zero mean flow as follow:

$$f_s^{eq} = w_{s,i} n_s \tag{10}$$

where the weights  $w_{s,i}$  depend on the lattice symmetry [31]. We can write

$$w_{s,i} = \begin{cases} z_s & i = 0\\ (1 - z_s)/2 & i = 1, 2, \end{cases}$$
 (11)

where  $z_s$  denotes the fraction of particles at rest and can be different for different species. For the reactive term  $\Omega_s^R$ , we use the simple isotropic form [31]

$$\Omega_s^R = w_{s,i}R_s, \tag{12}$$

where  $R_s$  is a non-linear reaction term and depends on the densities of the reacting species. Thus, it couples the Boltzmann equations for the different species. The choice given in Eq. (12) is the simplest choice that can provide the right macroscopic solution when using the LBM (as we shall see later).

To show that the lattice Boltzmann equation is valid for a reacting system, we employ a procedure called the Chapmann-Enskog expansion [17]. We first expand the left-hand side of Eq. 6 via a Taylor series:

$$f_{s}(\vec{x} + \vec{e_{i}}, i, t + 1) - f_{s}(\vec{x}, i, t),$$

$$\cong \frac{\partial f_{s}(\vec{x}, i, t)}{\partial t} + e_{i} \frac{\partial f_{s}(\vec{x}, i, t)}{\partial x} + \frac{1}{2} e_{i}^{2} \frac{\partial^{2} f_{s}(\vec{x}, i, t)}{\partial x^{2}},$$

$$= \Omega_{s}.$$
(13)

We then expand  $f_s$  about the equilibrium distribution function in terms of the parameter  $\varepsilon$ :

$$f_s \cong f_s^{eq} + \varepsilon f_s^{(1)} \tag{14}$$

We now assume [29]

$$\frac{\partial}{\partial x} \to \varepsilon \frac{\partial}{\partial x} \tag{15}$$

$$\frac{\partial}{\partial t} \to \varepsilon^2 \frac{\partial}{\partial t}$$
 (16)

$$R_s \to \varepsilon^2 R_s$$
 (17)

Substituting Eqs. (15), (16), and (17) into Eq. (13),

$$e_i \frac{\partial f_s^{eq}(\vec{x}, i, t)}{\partial x} = -\frac{f_s^{(1)}(\vec{x}, i, t)}{\tau_s}$$
 (18)

to order  $\varepsilon^1$  and

$$\frac{\partial f_s^{eq}(\vec{x}, i, t)}{\partial t} + e_i \frac{\partial f_s^{(1)}(\vec{x}, i, t)}{\partial x} + \frac{1}{2} e_i^2 \frac{\partial^2 f_s^{eq}(\vec{x}, i, t)}{\partial x^2} = w_{s,i} R_s$$
(19)

to order  $\varepsilon^2$ . From Eq. (18), we immediately obtain

$$f_s^{(1)}(\vec{x}, i, t) = -\tau_s w_{s,i} e_i \frac{\partial_s}{\partial_{\tau}}$$
 (20)

Inserting Eq. (20) to Eq. (19) and doing some simple algebra, we have, to order  $\varepsilon^2$ ,

$$\frac{\partial n_s}{\partial t} - (\tau_s - \frac{1}{2})e_i^2 \frac{\partial^2 n_s}{\partial x^2} = R_s \tag{21}$$

Eliminating the  $e_i^2$  term by carrying out an averaging with weight  $w_{s,i}$ , we get

$$\frac{\partial n_s}{\partial t} - (1 - Z_s)(\tau_s - \frac{1}{2})\frac{\partial^2 n_s}{\partial x^2} = R_s \tag{22}$$

which is the dimensionless version of the initial reaction-diffusion equation.

To summarize, we will now implement the numerical evaluation in two steps

· Collision step: 
$$\widetilde{f_s}(\vec{x},i,t+1) = f_s(\vec{x},i,t) - \frac{1}{\tau_s}[f_s - f_s^{eq}] + w_{s,i}R_s$$
 ,

Streaming step: 
$$f_s(\vec{x} + \vec{e_i}, i, t+1) = \tilde{f_s}(\vec{x}, i, t+1)$$

The boundary treatment is an important issue in the LBM simulation and advancement are still being made [32,33]. Here, we use the impermeable boundary suggested by Zhang et al. [34].

### III. NUMERICAL RESULTS AND DISCUSSION

To demonstrate the validity of the proposed LBM applied to the Howard dynamic model for determining the partition of E.~coli mediated by min proteins, we implemented the LBM as given in the previous section on a PC using C programming. In the simulation, we use the parameters given by Howard et~al. The 2-micronlong bacterium is divided into 250 grids. The discrete space steps are, therefore,  $dx=0.008~\mu\mathrm{m}$ . A time step of  $dt=6.410^{-5}$  s is chosen. The dimensionless param-

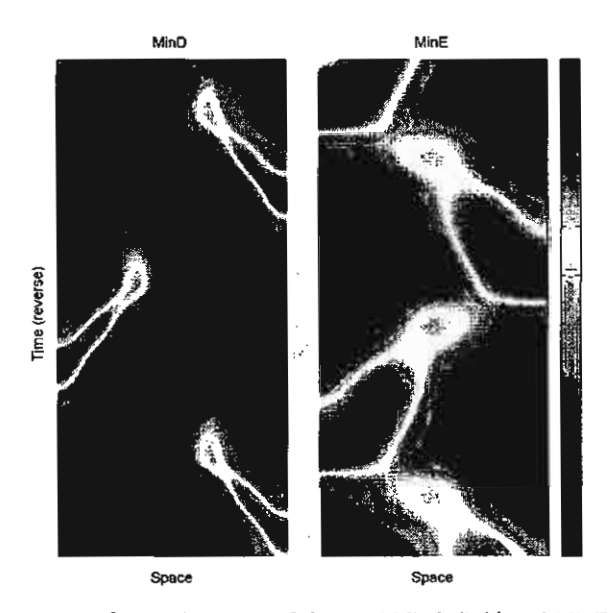


Fig. 1. Space-time plots of the total MinD (left) and MinE (right) densities. The color scale runs from the lowest (blue) to the highest (red). The MinD depletion from midcell and the MinE enhancement at midcell are immediately evident. Times increase from top to bottom, and the pattern repeats indefinitely as time increases. The vertical scale spans a time of 1000 second. The horizontal scale spans the bacteria's length (2  $\mu$ m).

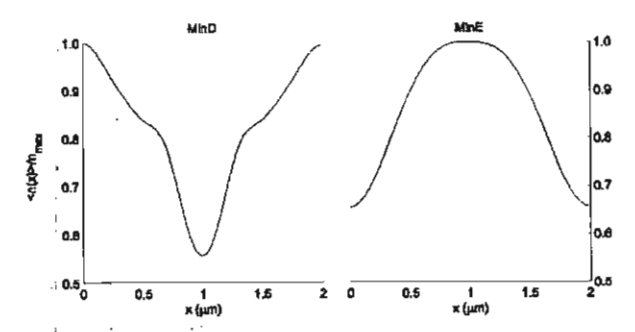


Fig. 2. Time-average MinD (left) and MinE (right) densities,  $< n(\chi) > /n_{max}$ , relative to their respective time-average maxima as functions of the position  $\chi$  (in  $\mu$ m) along the bacterium.

eters are  $D_D=0.28, D_E=0.6, D_d=D_e=0, \sigma_1=1.28\times 10^{-3}, \sigma_4=5.12\times 10^{-5}, \sigma_2=4.032\times 10^{-7}, \sigma_3=2.56\times 10^{-6}, \sigma_1=0.028,$  and  $\sigma_4=0.027.$  The relaxation time is calculated by using Eq. (22) and is given as  $\tau_s=D_s/(1-Z_s)+0.5.$  The initial number of MinD and MinE is randomly initialized as 3000 for  $n_D$  and 170 for  $n_E$ . Each simulation takes 156,250,000 iterations for  $10^4$  s of the time division of the bacterium. We test the system with two possible sets of the rest particle fraction,  $z_s=1/3$  and 2/3, for all species. We found that  $z_s=2/3$  gave the more accurate result. We now present some results to show the validity and the accuracy of our LBM and compare them with the results obtained from the deterministic reaction-diffusion equations.

In Fig. 1, the space-time plots of the MinD and the MinE concentrations for a cell of length 2  $\mu$ m are shown. They are in qualitative agreement with the simulation obtained by Howard et al. [26] and are in agreement with the experimental results. The MinE forms a line up in the middle of the cell and then sweeps towards a cell pole, displacing the MinD, which then reforms at the opposite pole. In Fig. 2, we plot the time-averaged MinD and MinE densities as functions of position. These are again in excellent agreement with those given by Howard et al. [26]. The results in both works are also in excellent agreement with the experimental data of Hale et al. [15]. The MinE concentration peaks at mid cell and has minimum at the cell rims, with MinD being virtually out of phase with MinE.

### IV. CONCLUDING REMARKS

In this paper, we have proposed a new LBM approach to investigate the dynamic pole-to-pole oscillations of *min* proteins used to determine the middle of bacterial cell division. We have developed a numerical scheme based on the LBM to simulate the coarse-grained coupled reaction-diffusion equations model used to describe the MinD/MinE interaction. It is found that our results

are in good agreement with those given by Howard et al. The results, in particular the oscillatory pattern of min proteins, are also in qualitative agreement with experimental results [35]. The LBM approach provides an alternative fast computational tool to study protein oscillation. We believe that the LBM is a useful scheme for simulating at the cellular level those biological system governed by the reaction-diffusion equations. In a future work, we will generalize the current LBM so that it can be used to study the effects of the inhomogeniety in the intracellular space and the possibility of asymmetrical cell division.

#### ACKNOWLEDGMENTS

We thank M. Howard, J. Wong-ekkabut, and M. Chooduang for their useful comments and suggestions. This research is supported in part by the Thailand Research Fund through grant numbers TRG4580090 and RTA4580005. The IRPUS Program 2547 assistance to Charin Modjung and W. Triampo is acknowledged. The support of the Development and Promotion of Science and Technology Talents program given to W. Ngamsaad is acknowledged. And The Office of Commission for Higher Education is also acknowledged.

### REFERENCES

- J. Lutkenhaus, Mol. Microbiol. 9, 403 (1993).
- [2] C. L. Woldringh, E. Mulder, P. G. Huls and N. Vischer, Res. Microbiol. 142, 309 (1991).
- [3] P. A. J. de Boer, R. E. Crossley and L. I. Rothfield, Cell 56, 641 (1989).
- [4] E. Mulder and C. L. Woldingh, J. Bacteriol. 171, 4303 (1989).
- [5] P. A. J. de Boer, R. E. Crossley and L. I. Rothfield, Proc. Natl. Acad. Sci. (USA) 87, 1129 (1990).
- [6] P. A. J. de Boer, R. E. Crossley, A. R. Hand and L. I. Rothfield, EMBO J. 10, 4371 (1991).
- [7] J. Huang, C. Cao and J. Lutkenhaus J. Bacteriol. 178, 5080 (1996).
- [8] Z. Hu and J. Lutkenhaus, Mol. Microbiol. 34, 82 (1999).
- [9] D. M. Raskin and P. A. J. de Boer, J. Bacteriol. 181, 6419 (1999).
- [10] X. Fu, Y-L. Shih, Y. Zhang and L. I. Rothfield, Proc. Natl. Acad. Sci. (USA) 98, 980 (2001).
- [11] D. M. Raskin and P. A. J. de Boer, Proc. Natl. Acad. Sci. (USA) 96, 4971 (1999).
- [12] S. L. Rowland, X. Fu, M. A. Sayed, Y. Zhang, W. R. Cook and L. I. Rothfield, J. Bacteriol. 182, 613 (2000).
- [13] K. C. Huang, Y. Meir and N. S. Wingreen, Proc. Natl. Acad. Sci. (USA) 100, 12724 (2003).
- [14] D. M. Raskin and P. A. J. de Boer, Cell 91 685 (1997).
- [15] C. A. Hale, H. Meinhardt and P. A. J. de Boer, EMBO J. 20, 1563 (2001).
- [16] R. Benzi, S. Succi and M. Vergassola, Phys. Rep. 222, 145 (1992).

- [17] S. Chen and G. D. Doolen, Ann. Rev. Fluid Mech. 30, 329 (1998).
- [18] Y. H. Qian, D. d'Humieres and P. A. Lallemand, Europhys. Lett. 17, 479 (1992).
- [19] H. Chen and S. Chen and W. H. Matthaeus, Phys. Rev. A 45, R5339 (1992).
- [20] N. S. Martys and H. D. Chen, Phys. Rev. E 53, 743 (1996).
- [21] G. D. Doolen, Lattice Gas Methods: Theory, Applications and Hardware, 2nd ed. (MIT, Cambridge, MA, 1991).
- [22] R. G. M. van der Sman and M. H. Ernst, J. Comput. Phys. 60, 766 (2000).
- [23] C. Migliorini, Y. H. Qian, H. Chen, E. Brown, R. Jainand and L. Munn, Biophys. J. 84, 1834 (2002).
- [24] C. H. Sun, C. Migliorini and L. Munn, Biophys. J. 85, 208 (2003).
- [25] M. Hirabayashi, M. Ohta, D. A. Rufenacht and B. Chopard, Future Gen. Comp. Sys. 20, 925 (2004).
- [26] M. Howard, A. D. Rutenberg and S. de Vet, Phys. Rev.

- Lett. 87, 278102 (2001).
- [27] G. Nicolis and I. Prigogine, Self Organization in Nonlinear Systems (Wiley, New York, 1977).
- [28] G. McNamara and G. Zanetti, Phys. Rev. Lett. 61, 2332 (1988).
- [29] S. P. Dawson, S. Chen and G. D. Doolen, J. Chem. Phys. 98, 1514 (1993).
- [30] P. L. Bhatnagar, E. P. Gross and M. Krook, Phys. Rev. 94, 511 (1954).
- [31] R. Blaak and P. M. Sloot, Comp. Phys. Comm. 129, 256 (2000).
- [32] S. Chen, D. O. Martinez and R. Mei, Phys. Fluids 8, 2527 (1996).
- [33] Q. Zou and X. He, Phys. Fluids 9, 6202 (1997).
- [34] X. Zhang, J. W. Crawford, A. G. Bengough and I. M. Young, Adv. Water Resour. 25, 601 (2002).
- [35] H. Meinhardt and P. A. J. de Boer, Proc. Natl. Acad. Sci. (USA) 98, 14202 (2001).

ij

ij

ij

## Modeling of the Dynamic Pole-to-Pole Oscillations of the Min Proteins in Bacterial Cell Division: the Effect of an External Field

Charin Modchang, Paisan Kanthang, Wannapong Triampo,\*
Waipot Ngamsaad, Narin Nuttawut and I-Ming Tang
Department of Physics and Capability Building Unit in Nanoscience and Nanotechnology,
Faculty of Science, Mahidol University, Bangkok 10400, Thailand

Suchitra Sanguansin, Ankana Boondirek and Yongwimol Lenbury

Department of Mathematics, Faculty of Science, Mahidol University, Bangkok 10400, Thailand

(Received 18 November 2004)

One of the most important steps in the developmental process of the bacteria cells at the cellular level is the determination of the middle of the cell and the proper placement of the septum, these being essential to the division of the cell. In E. coli, this step depends on the proteins MinC, MinD, and MinE. Exposure to a constant electric field may cause the bacteria's cell-division mechanism to change, resulting in an abnormal cytokinesis. To see the effects of an external field e.g., an electric or magnetic field on this process, we have solved a set of deterministic reaction diffusion equations, which incorporate the influence of an electric field. We have found some changes in the dynamics of the oscillations of the min proteins from pole to pole. The numerical results show some interesting effects, which are qualitatively in good agreement with some experimental results.

PACS numbers: 87.15.Aa, 87.17.Aa Keywords: External fields, Bacteria, E. coli, Cell division, Min proteins, MinCDE oscillation

### I. INTRODUCTION

Cell division is the process by which a cell separates into two new cells after its DNA has been duplicated and distributed into the two regions that will later become the future daughter cells. For a successful cell division to take place, the cell has to determine the optimal location of the cell separation and the time to start the cell cleavage. This involves the identification of the midpoint of the cell where the septum or cleavage furrow will form. For Escherichia coli (E. coli) and other rod-like bacteria, evidence has accumulated over the past few years which indicates that the separation into two daughter cells is achieved by forming a septum perpendicular to parent cell's long axis. To induce the separation, the FtsZ ring (Z ring), a tubulin-like GTPase, is believed to initiate and guide the septa growth by a process called contraction [1]. The Z ring is usually positioned close to the center, but it can also form in the vicinity of the cell poles. Two processes are known to regulate the placement of the division site: nucleoid occlusion [2] and the action of the min proteins [3]. Both processes interfere with the formation of the Z ring that determines the division site. Nucleoid occlusion is based on cytological evidence that indicates that the Z ring assembles preferentially on those portions of the membrane that do not directly surround the dense nucleoid mass [4].

The min proteins that control the placement of the division site are the MinC, the MinD, and the MinE proteins [3]. Experiments, involving the use of modified proteins show that inC is able to inhibit the formation of the FtsZ-ring [5]. MinD is an ATPase that is connected peripherally to the cytoplasmic membrane. It can bind to the MinC and activate the function of the MinC [6,7]. Recent studies show that MinD can also recruit MinC to the membrane. This suggests that MinD stimulates MinC by concentrating MinC near to its presumed site of activation [8,9]. MinE provides topological specificity to the division inhibitor [10]. Its expression results in a site-specific suppression of the MinC/MinD action so that FtsZ assembly is allowed at the middle of the cell, but is blocked at other sites [3]. In the absence of MinE, MinC/MinD is distributed homogeneously over the entire membrane. This results in a complete blockage of Z-ring formation. The long filamentous cells that are subsequently formed are not be able divide [8,9,11,12]. With fluorescent labeling, MinE was shown to attach to the cell wall only in the presence of MinD [13, 14]. As MinD dictates the location of MinC, the latter will oscillate by itself. This will result in a concentration of the division inhibitor at the membrane on either cell end, al-

<sup>\*</sup>E-mail: wtriampo@yahoo.com; Fax: 662-201-5843

ternating between being high or very low every other 20 s or so [8,9]. The presence of MinE is not only required for the MinC/MinD oscillation but also involved in setting the frequency of the oscillation cycle [11]. Several sets of evidence indicate that the MinE localization cycle is tightly coupled to the oscillation cycle of MinD.

Recent microscopy of the fluorescent labeled proteins involved in the regulation of *E. coli* division has uncovered stable and coherent oscillations (both spatial and temporal) of these three proteins [15]. The proteins oscillate from one end to the other end of the bacterium, moving between the cytoplasmic membrane and cytoplasm. The detail mechanism by which these proteins determine the correct position of the division plane is currently unknown, but the observed pole-to-pole oscillations of the corresponding distribution are thought to be of functional importance. Under different culture conditions and/or environment changes, e.g. pH, light, and external field, changes in the pole-to-pole oscillations can affect the growth of the bacteria. Here, we discuss only the effects of an electric field.

In the present work, we use a mathematical approach to investigate the influence of an external constant external field on cytokinesis mediated by pole-to-pole oscillations of the *min* protein. We propose a mathematical model and then solve it numerically to see how the *min* protein oscillation mechanism for bacteria cell division may change. We also present some comments about the connection between our mathematical approach and real-world experimental results.

### II. MODEL

Sets of reaction-diffusion equations have often been used in biological applications to model self-organization and pattern formation [16]. These mathematical equations have two components. The first component is the diffusion term that describes diffusion of the chemical species. At the molecular level, the diffusion term often results in a net flow of chemical species from regions of high concentration to regions of lower concentration. The second component is the reaction term that describes the self-organization of the biological systems.

We have adopted the dynamic model of compartmentization in the bacterial cell division process proposed by Howard [17] by adding an extra term that depends on the external electric field. The dynamics of bacteria in the presence of an external field is described by a set of four non-linear coupled reaction-diffusion equations. We focus on the  $E.\ coli$  bacteria, which are commonly studied rod-shaped bacteria of approximately  $2-6\ \mu m$  in length and around  $1-1.5\ \mu m$  in diameter.  $E.\ coli$  divides roughly every hour via cytokinesis. Our starting point is the set of one dimensional deterministic coupled reaction-diffusion equations describing the dynamics of the interactions between the local concentrations of the

MinD and the MinE proteins. The equations describe the time rates of change of the concentrations due to the diffusion of the MinD and the MinE and to transfer between the cell membrane and the cytoplasm. The dynamics of these *min* proteins in the presence of an external field, are described by

$$\frac{\partial \rho_D}{\partial t} = D_D \frac{\partial^2 \rho_D}{\partial x^2} + J_D \frac{\partial \rho_D}{\partial x} - \frac{\sigma_1 \rho_D}{1 + \sigma_1' \rho_e} + \sigma_2 \rho_e \rho_d, (1)$$

$$\frac{\partial \rho_d}{\partial t} = D_d \frac{\partial^2 \rho_d}{\partial x^2} + J_d \frac{\partial \rho_d}{\partial x} - \frac{\sigma_1 \rho_D}{1 + \sigma_1' \rho_e} - \sigma_2 \rho_e \rho_d, \quad (2)$$

$$\frac{\partial \rho_E}{\partial t} = D_E \frac{\partial^2 \rho_E}{\partial x^2} + J_E \frac{\partial \rho_E}{\partial x} - \sigma_3 \rho_D \rho_E - \frac{\sigma_4 \rho_e}{1 + \sigma_4' \rho_D} (3)$$

and

$$\frac{\partial \rho_e}{\partial t} = D_e \frac{\partial^2 \rho_e}{\partial x^2} + J_e \frac{\partial \rho_e}{\partial x} + \sigma_3 \rho_D \rho_E - \frac{\sigma_4 \rho_e}{1 + \sigma_4' \rho_D} \tag{4}$$

where  $\rho_D$  and  $\rho_E$  are the concentrations of the MinD and the MinE proteins in the cytoplasm, respectively, and  $\rho_d$  and  $\rho_e$  are the concentrations of the MinD and the MinE proteins on the cytoplasmic membrane. The first equation describes the time rate of change of the concentration of MinD  $(\rho_D)$  in the cytoplasm. The second is for the change in the MinD concentration  $(\rho_d)$  on the cytoplasmic membrane. The third is for the change of the concentration of MinE  $(\rho_E)$  in the cytoplasm. The last one is for the change in the MinE concentration  $(\rho_e)$  on the cytoplasmic membrane. Since the experimental results given Ref. 9, show that the MinC dynamics simply follows that of the MinD protein, we have not written out the equations for the MinC explicitly.

The important feature of our model is the second terms on the right-hand sides of the equations. They represent the effect of the external field in the reaction-diffusion equation [18,19] controlled by the external field parameter. We assume that a chemical substance moving in the region of an external field will experience a force that is proportional to the external field parameter J times the gradient of the concentration of that substance. In general,  $J = \mu E$ , where E is the field strength and  $\mu$ is the ionic mobility of the chemical substance.  $\mu$ , in general, will be proportional to the diffusion coefficient of the chemical substance and will depend on the total amount of free charge in that substance. In this model  $J_i = \mu_i E\{i = D, E, d, e\}$  is the external field parameter for each protein types. We assume that the diffusion coefficients  $\{D_D, D_E, D_d, D_e\}$  are isotropic and independent of x. The constant  $\sigma_1$  represents the association of MinD to the membrane wall [12].  $\sigma'_1$  corresponds to the membrane-bound MinE suppressing the recruitment of MinD from the cytoplasm.  $\sigma_2$  reflects the rate that the MinE on the membrane drives the MinD on the membrane into the cytoplasm. Based on evidence for the cytoplasmic interaction between MinD and MinE [7], we let  $\sigma_3$  be the rate that cytoplasmic MinD recruits cytoplasmic MinE to the membrane and  $\sigma_4$  be the rate of dissociation of MinE from the membrane to the cytoplasm. Finally,  $\sigma_4'$  corresponds to the cytoplasmic MinD suppressing the release of the membrane-bound MinE. Evidence points to most of the diffusion process occurring in the cytoplasm. It is, therefore, reasonable to set  $D_d$  and  $D_e$  to zero. It follows immediately that  $\mu_d = \mu_e = 0$  and  $J_d = J_e = 0$ 

In our model, we assume that the total number of each type of protein is conserved. We further assume that the *min* proteins can bind/unbind from the membrane and that the proteins do not degrade during the process. The zero-flux boundary conditions are imposed at both ends of the bacterium. The total amounts of MinD and MinE, obtained by integrating  $\rho_D + \rho_d$  and  $\rho_E + \rho_e$  over the length of the bacterium, are conserved.

### III. NUMERICAL RESULTS AND DISCUSSION

Since the bacterium length is very short, it is reasonable to assume that the applied electric field has a constant value throughout the bacterium length. We have numerically solved the set of four coupled reactiondiffusion equations, Eqs. (1)-(4), by using the explicit Euler method [20]. The length of the E. coli is taken to be 2  $\mu m$ . The total time needed for each simulation is approximately 104 s. In our simulations, we have discretized space and time; i.e., we have taken  $dx = 8 \times 10^{-3} \ \mu \text{m}$  and  $dt = 1 \times 10^{-5} \ \text{s}$ . The space covering the bacterium is divided into 251 grid points, and the time is divided into 109 times steps (109 iteration steps). Initially, we assume that MinD and MinE are mainly at the opposite ends of the bacterium with the number of min molecules in each cell being 3000 for the MinD population [6] and 170 for the MinE population [21]. Since the total amount of MinD and MinE in E. coli must be conserved, we set the flux of MinD and MinE to zero at both ends of the bacterium. Since there are no experimental values of  $\mu$  for either MinD and MinE, we work with the external field parameter J, which is proportional to E, instead of E explicitly. We also assume that  $\mu_D = \mu_E$  (we assume MinD and MinE have the same type of charges). It follows immediately that  $J_D=J_E\equiv J$ . The values of the other parameters are:  $D_D = 0.28 \ \mu\text{m}^2\text{s}^{-1}$ ,  $D_E = 0.6 \ \mu\text{m}^2\text{s}^{-1}$ ,  $\sigma_1 = 20 \ \text{s}^{-1}$ ,  $\sigma_1 = 0.028 \ \mu\text{m}$ ,  $\sigma_2 = 0.0063 \ \mu\text{m}^{-1}$ ,  $\sigma_3 = 0.04 \ \mu\text{m}^{-1}$ ,  $\sigma_4 = 0.8 \ \text{s}^{-1}$ , and  $\sigma_4 = 0.027 \ \mu\text{m}$ . In our analyses of the numerical results, we looked at the time-averaged values of the concentrations of MinD and MinE and at the patterns of the oscillations of MinD and MinE for various Jvalues.

In the absent of an external field, the numerical results [17] show that most of the MinD will be concentrated at the membrane and the MinE at mid cell. This results in

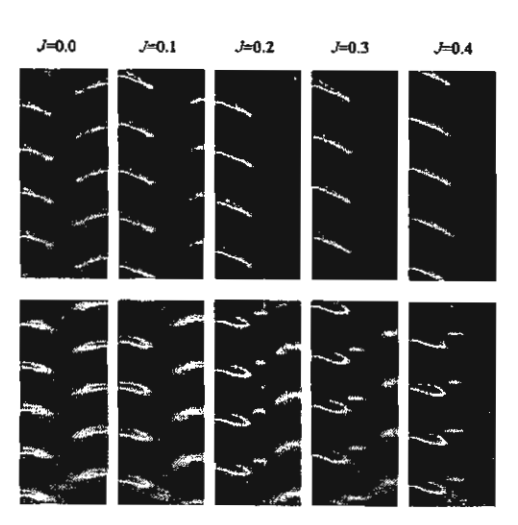


Fig. 1. Space-time plots of the total  $(\sigma_D + \sigma_d)$  MinD (above) and total  $(\sigma_E + \sigma_e)$  MinE (below) concentration for J=0.0 m/s to J=0.4 m/s. The color scale, running from blue to red, denotes an increase in the concentration from the lowest to the highest. The MinD depletion from mid cell and the MinE enhancement at the mid cell are immediately seen. The vertical scale spans time for 500 s. The times increase from bottom to top, and the oscillations pattern repeats infinitely as time increases. The horizontal scale spans the bacterial length  $(2~\mu m)$ . Note the increase in the MinD and MinE concentrations at the left end of the bacterium as J increases.

an accurate division at mid cell. In the presence of an external field, both MinD and MinE experience a force in the same direction. This force causes a shift of the time-averaged minimum of MinD. This shifts the division site from mid cell. Our numerical solutions show that the behavior of the Min system in the presence of an external field depends on the strength of the external field parameter J.

Figure 1 shows the oscillation patterns for  $J_E = J_D \equiv J = 0.0$  m/s to J = 0.4 m/s. It is seen that as J increase, both the MinD and the MinE concentrations in the left part of the E. coli become larger while the two concentrations in the right part become smaller as J is increased. This behavior is a reflection of the fact that the external force is acting in the left direction. These patterns show a shifting in the concentrations of the min proteins towards the left pole.

In Figure 2, we show the time-averaged concentrations of the MinD and the MinE proteins at different positions within the bacteria. In these curves, positive values of the external field parameter are used. From this Figure, we see that in the case of no external field ( $J=0.0~\rm m/s$ ), the time-averaged concentrations of MinD and MinE are symmetric about mid cell. MinD has a minimum at mid cell while MinE has a maximum. When an external field is applied, we see a shift in the minima of MinD and in the maxima of MinE. The time-averaged concentration

Journal of the Korean Physical Society, Vol. 46, No. 4, April 2005

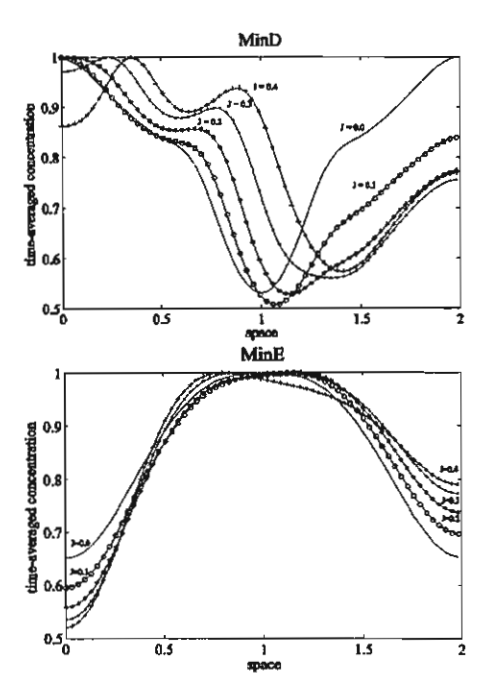


Fig. 2. Time-averaged concentration of MinD (above) and MinE (below) relative to their respective time-averaged maxima,  $\langle \sigma(x) \rangle / \sigma_{max}$ , as a function of the position x (in  $\mu$ m) along the bacterium axis under the influence of positive values of a static external field. The curves show a shift in the local minima of the MinD and the local maxima of the MinE from the mid cell that depends on the strength of the field.

curves are no longer symmetric about mid cell. In nature, the MinE protein looks like a ring structure that effectively positions the anti-MinCD activity [11,14]. MinCD inhibits the division process, so in nature, the bacterium divides at the site where the minimum MinD concentration occurs. The value of the MinE concentration is not maximum at the mid cell. The minimum of the MinD shifts to the right pole under the influence of positive J values.

We have measured the percent of shifting of the timeaveraged concentration in the local minima of MinD and the local maxima of MinE. This is shown in Fig. 3. The figure shows that the minimum of MinD is always shifted to the right pole. This is the result of the external force pulling MinD to the left. The maximum of MinE is not always shifted to the right. When J < 0.2 m/s, the maximum of MinE is shifted to the right, but when J > 0.2 m/s, it shifted to the left of mid cell. This difference arises because of the relative magnitudes of the forces acting on the two proteins. First of all, there is an internal force between the MinD and the MinE proteins. This force causes MinE to repel MinD. In the absence of any other forces, this explains why the location of the maximum of MinE is the location of the minimum of MinD. When an external field is applied (as expressed by a non-zero value of J), then one must take into account

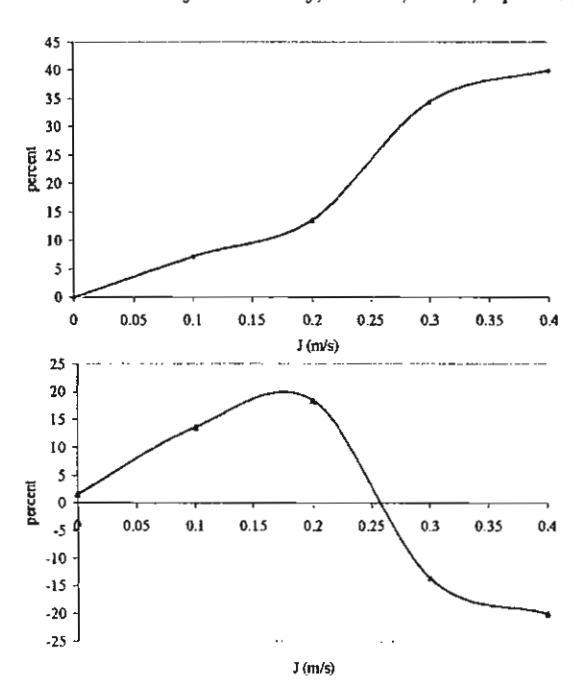


Fig. 3. Percents of the shifting of the local minima of MinD (above) and the local maxima of MinE (below) from mid cell for various values of J. Positive values denote a shift to the right pole and a negative value to the left pole.

the relative magnitudes of the two forces.

When J is large (larger than 2 m/s), the external force dominates the internal force between the MinD and the MinE proteins. The external force pulls MinD and MinE in the same direction, causing the location of the maximum of MinE to be no longer at the location of the minimum of MinD. If J is small (smaller than 0.2 m/s), the internal force between MinD and MinE dominates. This results in the two location (the maximum of MinE and the minimum of MinD) to be nearly the same. In Fig. 3, we also see that the shifts of the minimum of the MinD concentrations increase as the field parameter J increases. Since the division site will be the location where the MinD concentration is minimum, the shift in the minimum of MinD concentration to the right pole indicates that the division site must also shift to the right pole. When we let J be negative, the results are very similar to those for positive J values, as expected; the curves for the time averages of the concentrations of the min proteins shift in the mirror side about mid cell.

In Figs. 4(a) and 4(b), we show the concentrations of the MinD and the MinE proteins at the left end grid, the middle grid, and the right end grid versus time. In these figures, it is easy to see that when J = 0.0 m/s, the concentrations of MinD (or MinE) at the left end grid and the right end grid have the same patterns of oscillation with the same frequencies and amplitudes, but with a phase difference of 180°. At the mid cell grid, the frequency of the oscillation is two times greater than that

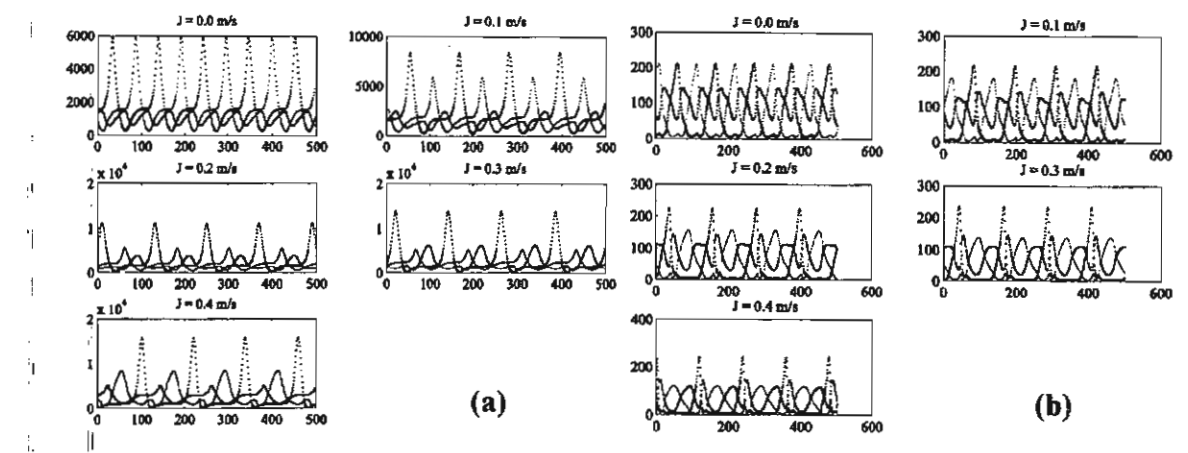


Fig. 4. (a) Plots of the concentration of MinD at the the left end grid (+), the middle grid (x), and the right end grid (·) versus time in seconds for J=0.0 m/s to J=0.4 m/s. The vertical scales denote concentration in molecules per meter. (b) Plots of the concentration of MinE at the left end grid (+), the middle grid (x), and the right end grid (·) as functions of time in seconds for J=0.0 m/s to J=0.4 m/s. The vertical scales denote concentration in molecules per meter.

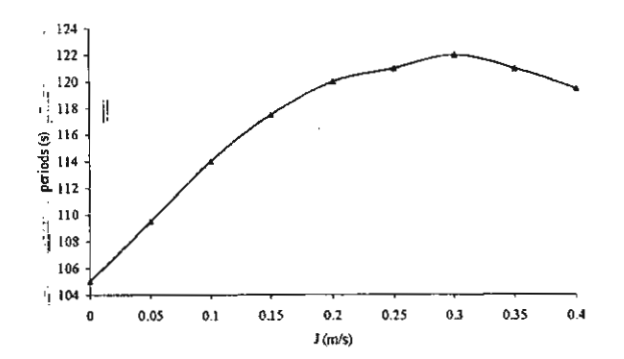


Fig. 5. Plots of the concentration of MinE at the left end grid (+), the middle grid (x), and the right end grid (·) as functions of time in seconds for J = 0.0 m/s to J = 0.4 m/s. The vertical scales denote concentration in molecules per meter.

of right end grid. When an external field is applied, the amplitudes of the oscillations at the two end grids are no longer equal, but the frequencies of the oscillations of the three grids become the same. As J is increased, the amplitude of the oscillation at the right end grid is seen to decrease while those of the left end and mid cell grids are seen to increase.

Figure 5 show the periods of oscillation for the MinD concentration at the left end grid for various value of J. In this figure, we see that for the case of no external field, the period of the oscillation is equal to 115 s, which is in good agreement with the experimental value. When an external field is applied, the period of the oscillation is seen to increase. When J is not too large (J < 0.3), the period of the oscillation increases as J is increased. The increase in the period of oscillation as an external field is applied indicates that in the presence of an external

field, the bacterium needs a longer time to divide.

### IV. CONCLUDING REMARKS

Proper divisions of bacteria require accurate definition of the division site [3]. This accurate identification of the division site is determined by the rapid pole-to-pole oscillations of MinCDE [8,11,22]. Using a mathematical model to describe the dynamics of the *min* pole-to-pole oscillations, Howard *et al.* [17] found that the mid cell position in the *Escherichia coli* bacteria corresponded to the point where the time-averaged MinD and MinE concentrations were minimum and maximum, respectively. They also found that the concentrations of these two proteins were symmetric about the mid cell position.

To see the effect of exposing E. coli bacteria to an electric field, we have added some additional terms to the reaction-diffusion equations for the pole-to-pole oscillations proposed by Howard et al for the min proteins in the E. coli bacteria. The additional terms are the gradient terms appearing in Eqs.(1)-(4). These terms depend on the strength of the external field and the charge of the protein. We then used a numerical scheme to solve the resulting coarse-grained coupled reaction-diffusion equations. The results are shown in Figs. 1 to 5. Our results shows deviations from the results obtained by Howard et al., e.g.: the concentrations of MinD and MinE are no longer symmetric about the middle of the long axis, nor are the minimum and the maximum of the MinD and the MinE concentrations at the middle of the long axis. The shift in the minimum of the time-averaged concentration of MinD from mid cell should shift the division site. The shift of the minimum concentration of MinD from the midpoint appears to depend on the strength of the external field. This indicates that if the parent cell can divide under these condition, it must divide into two filamentous cells, providing the external field is strong enough. Since an external field can shift the minimum of the time-averaged concentration of MinD, an external electric field can interfere with the division process.

### ACKNOWLEDGMENTS

We thank M. Howard, J. Wong-ekkabut, and M. Chooduang for their useful comments and suggestions. This research is supported in part by the Thailand Research Fund through grant numbers TRG4580090 and RTA4580005, and the Commission on Higher Education. The support of the Industrial and Research Projects for Undergraduate Students Program 2547 given to Charin Modchang and W. Triampo is acknowledged, as is the support of the Development and Promotion of Science and Technology Talents program given to Waipot Ngamsaad.

### REFERENCES

- [1] J. Lutkenhaus, Mol. Microbiol. 9, 403 (1993).
- [2] C. L. Woldringh, E. Mulder, P. G. Huls and N. Vischer, Res. Microbiol. 142, 309 (1991).
- [3] P. A. J. de Boer, R. E. Crossley and L. I. Rothfield, Cell. 156, 4303 (1989).
- [4] E. Mulder and C. L. J. Woldingh, Bacteriol. 171, 4303 (1989).
- [5] P. A. J. de Boer, R. E. Crossley and L. I. Rothfield, Proc. Natl. Acad. Sci. USA 87, 1129 (1990).

- [6] P. A. J. de Boer, R. E. Crossley, A. R. Hand and L. I. Rothfield, EMBO J. 10, 4371 (1991).
- [7] J. Huang, C. Cao and J. Lutkenhaus, J. Bacteriol. 178, 5080 (1996).
- [8] Z. Hu and J. Lutkenhaus, J. Mol. Microbiol. 34, 82 (1999).
- [9] D. M. Raskin and P. A. J. de Boer, J. Bacteriol. 181, 6419 (1999).
- [10] X. Fu, Y-L. Shih, Y. Zhang and L. I. Rothfield, Proc. Natl. Acad. Sci. USA 98, 980 (2001).
- [11] D. M. Raskin and P. A. J. de Boer, Proc. Natl. Acad. Sci. USA 96, 4971 (1999).
- [12] S. L. Rowland, X. Fu, M. A. Sayed, Y. Zhang, W. R. Cook and L. I. Rothfield, J. Bacteriol. 182, 613 (2000).
- [13] K. C. Huang, Y. Meir and N. S. Wingreen, Proc. Natl. Acad. Sci. USA 100, 12724 (2003).
- [14] D. M. Raskin and P. A. J. de Boer, Cell. 91, 685 (1997).
- [15] C. A. Hale, H. Meinhardt and P. A. J. de Boer, EMBO J. 20, 1563 (2001).
- [16] G. Nicolis and I. Prigogine, Self Organization in Nonlinear Systems (Wiley, New York, 1977).
- [17] M. Howard, A. D. Rutenberg and S. de Vet, Phys. Rev. Lett. 87, 278102 (2001).
- [18] E. P. Zemskov, V. S. Zykov, K. Kassner and S. C. Müller, Physica D. 183, 117 (2003).
- [19] A. P. Munuzuri, V. A. Davydov, V. Perez-Munuzuri, M. Gomez-Gesteira and V. Perez-Villar, Chaos, Solitons & Fractals 7, 585 (1995).
- [20] W. H. Press, S. A. Teukolsky, W. T. Vetterling and B. P. Flannery Numerical Recipes in C++: The Art of Scientific Computing (Cambridge University Press, 2002).
- [21] C-R. Zhao, P. A. J. de Boer and L. I. Rothfield, Proc. Natl. Acad. Sci. USA. 92, 4313 (1995).
- [22] H. Meinhardt and P. A. J. de Boer, Proc. Natl. Acad. Sci. USA 98, 14202 (2001).

## A NOTE ON ASYMPTOTIC STABILITY CONDITIONS FOR DELAY DIFFERENCE EQUATIONS

T. KAEWONG, Y. LENBURY, AND P. NIAMSUP

Received 26 May 2004 and in revised form 27 February 2005

We obtain necessary and sufficient conditions for the asymptotic stability of the linear delay difference equation  $x_{n+1} + p \sum_{j=1}^{N} x_{n-k+(j-1)l} = 0$ , where n = 0, 1, 2, ..., p is a real number, and k, l, and N are positive integers such that k > (N-1)l.

### 1. Introduction

In [4], the asymptotic stability condition of the linear delay difference equation

$$x_{n+1} - x_n + p \sum_{j=1}^{N} x_{n-k+(j-1)l} = 0,$$
 (1.1)

where  $n \in \mathbb{N}_0 = \mathbb{N} \cup \{0\}$ , p is a real number, and k, l, and N are positive integers with k > (N-1)l is given as follows.

THEOREM 1.1. Let k, l, and N be positive integers with k > (N-1)l. Then the zero solution of (1.1) is asymptotically stable if and only if

$$0 
(1.2)$$

where M = 2k + 1 - (N - 1)l.

Theorem 1.1 generalizes asymptotic stability conditions given in [1, page 87], [2, 3, 5], and [6, page 65]. In this paper, we are interested in the situation when (1.1) does not depend on  $x_n$ , namely we are interested in the asymptotic stability of the linear delay difference equation of the form

$$x_{n+1} + p \sum_{j=1}^{N} x_{n-k+(j-1)l} = 0, (1.3)$$

where  $n \in \mathbb{N}_0 = \mathbb{N} \cup \{0\}$ , p is a real number, and k, l, and N are positive integers with  $k \ge (N-1)l$ . Our main theorem is the following.

Copyright © 2005 Hindawi Publishing Corporation International Journal of Mathematics and Mathematical Sciences 2005:7 (2005) 1007–1013 DOI: 10.1155/IJMMS.2005.1007

### 1008 A note on asymptotic stability conditions

THEOREM 1.2. Let k, l, and N be positive integers with  $k \ge (N-1)l$ . Then the zero solution of (1.3) is asymptotically stable if and only if

$$-\frac{1}{N}$$

where  $p_{min}$  is the smallest positive real value of p for which the characteristic equation of (1.3) has a root on the unit circle.

### 2. Proof of theorem

The characteristic equation of (1.3) is given by

$$F(z) = z^{k+1} + p(z^{(N-1)l} + \dots + z^{l} + 1) = 0.$$
 (2.1)

For p = 0, F(z) has exactly one root at 0 of multiplicity k + 1. We first consider the location of the roots of (2.1) as p varies. Throughout the paper, we denote the unit circle by C and let M = 2k + 2 - (N - 1)l.

Proposition 2.1. Let z be a root of (2.1) which lies on C. Then the roots z and p are of the form

$$z = e^{w_{m}i}, (2.2)$$

$$p = (-1)^{m+1} \frac{\sin(lw_m/2)}{\sin(Nlw_m/2)} \equiv p_m \tag{2.3}$$

for some m = 0, 1, ..., M - 1, where  $w_m = (2m/M)\pi$ . Conversely, if p is given by (2.3), then  $z = e^{w_m i}$  is a root of (2.1).

Proof. Note that z=1 is a root of (2.1) if and only if p=-1/N, which agrees with (2.2) and (2.3) for  $w_m=0$ . We now consider the roots of (2.1) which lie on C except the root z=1. Suppose that the value z satisfies  $z^{Nl}=1$  and  $z^l\neq 1$ . Then  $z^{Nl}-1=(z^l-1)(z^{(N-1)l}+\cdots+z^l+1)=0$  which gives  $z^{(N-1)l}+\cdots+z^l+1=0$ , and hence z is not a root of (2.1). As a result, to determine the roots of (2.1) which lie on C, it suffices to consider only the value z such that  $z^{Nl}\neq 1$  or  $z^l=1$ . For these values of z, we may write (2.1) as

$$p = -\frac{z^{k+1}}{z^{(N-1)l} + \dots + z^l + 1}. (2.4)$$

Since p is real, we have

$$p = -\frac{\overline{z}^{k+1}}{\overline{z}^{(N-1)l} + \dots + \overline{z}^l + 1} = -\frac{z^{-k-1+(N-1)l}}{z^{(N-1)l} + \dots + z^l + 1},$$
 (2.5)

where  $\overline{z}$  denotes the conjugate of z. It follows from (2.4) and (2.5) that

$$z^{2k+2-(N-1)l} = 1 (2.6)$$

which implies that (2.2) is valid for m = 0, 1, ..., M - 1 except for those integers m such that  $e^{Nlw_m i} = 1$  and  $e^{lw_m i} \neq 1$ . We now show that p is of the form stated in (2.3). There are two cases to be considered as follows.

Case 1. z is of the form  $e^{w_m i}$  for some m = 1, 2, ..., M - 1 and  $z^{Nl} \neq 1$ . From (2.4), we have

$$p = -\frac{z^{k+1}(z^{l}-1)}{z^{Nl}-1} = -\frac{e^{(k+1)w_{m}i}(e^{lw_{m}i}-1)}{e^{Nlw_{m}i}-1}$$

$$= -\frac{e^{(k+1-(N-1)(l/2))w_{m}i}(e^{lw_{m}i/2}-e^{-lw_{m}i/2})}{e^{Nlw_{m}i/2}-e^{-Nlw_{m}i/2}}$$

$$= -e^{(k+1-(N-1)(l/2))w_{m}i}\frac{\sin(lw_{m}/2)}{\sin(Nlw_{m}/2)}$$

$$= -e^{m\pi i}\frac{\sin(lw_{m}/2)}{\sin(Nlw_{m}/2)} = (-1)^{m+1}\frac{\sin(lw_{m}/2)}{\sin(Nlw_{m}/2)} = p_{m}.$$
(2.7)

Case 2. z is of the form  $e^{w_m i}$  for some m = 1, 2, ..., M - 1 and  $z^l = 1$ .

In this case, we have  $lw_m = 2q\pi$  for some positive integer q. Then taking the limit of  $p_m$  as  $lw_m \to 2q\pi$ , we obtain

$$p = -\frac{(-1)^{m+q(N-1)}}{N}. (2.8)$$

From these two cases, we conclude that p is of the form in (2.3) for m = 1, 2, ..., M - 1 except for those m such that  $e^{Nlw_m i} = 1$  and  $e^{lw_m i} \neq 1$ .

Conversely, if p is given by (2.3), then it is obvious that  $z = e^{w_m t}$  is a root of (2.1). This completes the proof of the proposition.

From Proposition 2.1, we may consider p as a holomorphic function of z in a neighborhood of each  $z_m$ . In other words, in a neighborhood of each  $z_m$ , we may consider p as a holomorphic function of z given by

$$p(z) = -\frac{z^{k+1}}{z^{(N-1)l} + \dots + z^l + 1}.$$
 (2.9)

Then we have

$$\frac{dp(z)}{dz} = -\frac{(k+1)z^k}{z^{(N-1)l} + \dots + z^l + 1} + \frac{z^k \{(N-1)lz^{(N-1)l} + \dots + lz^l\}}{\left(z^{(N-1)l} + \dots + z^l + 1\right)^2}.$$
 (2.10)

From this, we have the following lemma.

LEMMA 2.2.  $dp/dz|_{z=e^{mmi}} \neq 0$ . In particular, the roots of (2.1) which lie on C are simple.

*Proof.* Suppose on the contrary that  $dp/dz|_{z=e^{w_{mi}}}=0$ . We divide (2.10) by p(z)/z to obtain

$$k+1-\frac{l\{(N-1)z^{(N-1)l}+\cdots+z^l\}}{z^{(N-1)l}+\cdots+z^l+1}=0.$$
 (2.11)

Substituting z by  $1/\overline{z}$  in (2.10), we obtain

$$k+1-\frac{l\{(N-1)+(N-2)z^l+\cdots+z^{(N-2)l}\}}{z^{(N-1)l}+\cdots+z^l+1}=0.$$
 (2.12)

### 1010 A note on asymptotic stability conditions

By adding (2.11) and (2.12), we obtain

$$2k + 2 - (N - 1)l = 0 (2.13)$$

which contradicts  $k \ge (N-1)l$ . This completes the proof.

From Lemma 2.2, there exists a neighborhood of  $z = e^{w_{m}i}$  such that the mapping p(z) is one to one and the inverse of p(z) exists locally. Now, let z be expressed as  $z = re^{i\theta}$ . Then we have

$$\frac{dz}{dp} = \frac{z}{r} \left\{ \frac{dr}{dp} + ir \frac{d\theta}{dp} \right\}$$
 (2.14)

which implies that

$$\frac{dr}{dp} = \text{Re}\left\{\frac{r}{z}\frac{dz}{dp}\right\} \tag{2.15}$$

as p varies and remains real. The following result describes the behavior of the roots of (2.1) as p varies.

PROPOSITION 2.3. The moduli of the roots of (2.1) at  $z = e^{w_m i}$  increase as |p| increases.

*Proof.* Let r be the modulus of z. Let  $z = e^{w_m i}$  be a root of (2.1) on C. To prove this proposition, it suffices to show that

$$\left. \frac{dr}{dp} \cdot p \right|_{z=e^{i\nu_{in}i}} > 0. \tag{2.16}$$

There are two cases to be considered.

Case 1  $(z^{NI} \neq 1)$ . In this case, we have

$$p(z) = -\frac{z^{k+1}(z^{l}-1)}{z^{Nl}-1} = -\frac{z^{k}f(z)}{z^{Nl}-1},$$
(2.17)

where  $f(z) = z(z^l - 1)$ . Then

$$\frac{dp}{dz} = -\frac{z^{k-1}g(z)}{(z^{NI}-1)^2},\tag{2.18}$$

where  $g(z) = (kf(z) + zf'(z))(z^{Nl} - 1) - Nlz^{Nl}f(z)$ . Letting  $w(z) = -(z^{Nl} - 1)^2/(z^kg(z))$ , we obtain

$$\frac{dr}{dp} = \operatorname{Re}\left(\frac{r}{z}\frac{dz}{dp}\right) = r\operatorname{Re}(w). \tag{2.19}$$

We now compute Re(w). We note that

$$f(\overline{z}) = -\frac{f(z)}{z^{l+2}}, \qquad f'(\overline{z}) = \frac{h(z)}{z^l}, \tag{2.20}$$

T. Kaewong et al. 1011

where  $h(z) = l + 1 - z^{l}$ . From the above equalities and as  $z^{M} = 1$ , we have

$$\overline{z}^{k}g(\overline{z}) = \frac{1}{z^{k}} \left\{ \left( kf(\overline{z}) + \frac{1}{z}f'(\overline{z}) \right) \left( \frac{1}{z^{Nl}} - 1 \right) - \frac{Nl}{z^{Nl}} f(\overline{z}) \right\} 
= \frac{\left( - kf(z) + zh(z) \right) \left( 1 - z^{Nl} \right) + Nlf(z)}{z^{Nl+l+2+k}} 
= \frac{\left( - kf(z) + zh(z) \right) \left( 1 - z^{Nl} \right) + Nlf(z)}{z^{2Nl-k}}.$$
(2.21)

It follows that

$$Re(w) = \frac{w + \overline{w}}{2}$$

$$= -\frac{1}{2} \left\{ \frac{(z^{Nl} - 1)^{2}}{z^{k} g(z)} + \frac{(\overline{z}^{Nl} - 1)^{2}}{\overline{z}^{k} g(\overline{z})} \right\}$$

$$= -\frac{1}{2} \left\{ \frac{\overline{z}^{k} g(\overline{z}) (z^{Nl} - 1)^{2} + z^{k} g(z) (\overline{z}^{Nl} - 1)^{2}}{|g(z)|^{2}} \right\}$$

$$= -\frac{1}{2 |g(z)|^{2}} \left\{ \frac{(-kf(z) + zh(z)) (1 - z^{Nl}) + Nlf(z)}{z^{2Nl - k}} \cdot (z^{Nl - 1})^{2} + z^{k} ((kf(z) + zf'(z)) (z^{Nl} - 1) - Nlz^{Nl} f(z)) (\frac{1}{z^{Nl}} - 1)^{2} \right\}$$

$$= -\frac{(z^{Nl} - 1)^{2} z^{k}}{2z^{2Nl} |g(z)|^{2}} \left\{ (kf(z) - zh(z)) (z^{Nl} - 1) + Nlf(z) + ((kf(z) + zf'(z)) (z^{Nl} - 1)) - Nlz^{Nl} f(z) \right\}$$

$$= -\frac{(z^{Nl} - 1)^{3} z^{k}}{2z^{2Nl} |g(z)|^{2}} \left\{ 2kf(z) + z(f'(z) - h(z)) - Nlf(z) \right\}. \tag{2.22}$$

Since

$$2kf(z) + z(f'(z) - h(z)) - Nlf(z) = Mf(z),$$
 (2.23)

we obtain

$$\operatorname{Re}(w) = \frac{(z^{Nl} - 1)^4 M}{2z^{2Nl} |g(z)|^2} \cdot \frac{-z^k f(z)}{z^{Nl} - 1} = \frac{(z^{Nl} - 1)^4 M p}{2z^{2Nl} |g(z)|^2}.$$
 (2.24)

The value of Re(w) at  $z = e^{iv_m i}$  is

$$Re(w) = \frac{(z^{Nl} - 1)^4}{z^{2Nl}} \cdot \frac{Mp}{2|g(z)|^2} = (2\cos Nlw_m - 2)^2 \cdot \frac{Mp}{2|g(z)|^2} > 0.$$
 (2.25)

### 1012 A note on asymptotic stability conditions

Therefore,

$$\frac{dr}{dp} = \frac{2r(\cos Nlw_m - 1)^2 Mp}{|g(z)|^2}$$
 (2.26)

and it follows that (2.16) holds at  $z = e^{w_m i}$ .

Case 2 ( $z^l = 1$ ). With an argument similar to Case 1, we obtain

$$\frac{dr}{dp} = \frac{2rN^2Mp}{\left| (M+1)z - M + 1 \right|^2}$$
 (2.27)

which implies that (2.16) is valid for  $z = e^{i v_m i}$ .

This completes the proof.

We now determine the minimum of the absolute values of  $p_m$  given by (2.3). We have the following result.

PROPOSITION 2.4.  $|p_0| = \min\{|p_m| : m = 0, 1, ..., M-1\}$ .

To prove Proposition 2.4, we need the following lemma, which was proved in [4].

LEMMA 2.5. Let N be a positive integer, then

$$\left|\frac{\sin Nt}{\sin t}\right| \le N \tag{2.28}$$

holds for all  $t \in \mathbb{R}$ .

Proof of Proposition 2.4. From (2.3),  $p_m = (-1)^{m+1} (\sin(lw_m/2)/\sin(Nlw_m/2))$ . For m = 0, it follows from L'Hospital's rule that  $p_0 = -1/N$ . For m = 1, 2, ..., M-1, we have

$$|p_m| = \left| (-1)^{m+1} \frac{\sin(lw_m/2)}{\sin(Nlw_m/2)} \right| \ge \frac{1}{N}$$
 (2.29)

by Lemma 2.5. This completes the proof.

We are now ready to prove Theorem 1.2.

Proof of Theorem 1.2. Note that  $F(1) = 1 + Np \le 0$  if and only if  $p \le -1/N$ . Since  $\lim_{z \to +\infty} F(z) = +\infty$ , it follows that (2.1) has a positive root  $\alpha$  such that  $\alpha > 1$  when  $p \le -1/N$ . We claim that if |p| is sufficiently small, then all the roots of (2.1) are inside the unit disk. To this end, we note that when p = 0, (2.1) has exactly one root at 0 of multiplicity k + 1. By the continuity of the roots with respect to p, this implies that our claim is true. By Proposition 2.4,  $p_0 = -1/N$  and  $|p_m| \ge 1/N$  which implies that  $|p_0| = 1/N$  is the smallest positive value of p such that a root of (2.1) intersects the unit circle as |p| increases. Moreover, Proposition 2.3 implies that if  $p > p_{\min}$ , then there exists a root  $\alpha$  of (2.1) such that  $|\alpha| \ge 1$ , where  $p_{\min}$  is the smallest positive real value of p for which (2.1) has a root on C. We conclude that all the roots of (2.1) are inside the unit disk if and only if -1/N . In other words, the zero solution of (1.3) is asymptotically stable if and only if condition (1.4) holds. This completes the proof.

### 3. Examples

Example 3.1. In (1.3), Let l and k be even positive integers, then we have

$$F(-1) = -1 + pN. (3.1)$$

Thus if p = 1/N, then F(-1) = 0 and we conclude that (1.3) is asymptotically stable if and only if -1/N .

Example 3.2. In (1.3), let N=3, l=3, and k=6. Then M=8 and we obtain  $p_0=-1/3$ ,  $p_1=\sin(3/8)\pi/\sin(9/8)\pi$ ,  $p_2=-\sin(3/4)\pi/\sin(9/4)\pi$ ,  $p_3=\sin(9/8)\pi/\sin(27/8)\pi$ ,  $p_4=-\sin(3/2)\pi/\sin(9/2)\pi$ ,  $p_5=\sin(15/8)\pi/\sin(45/8)\pi$ ,  $p_6=-\sin(9/4)\pi/\sin(27/4)\pi$ , and  $p_7=\sin(21/8)\pi/\sin(63/8)\pi$ . Thus,  $p_3=p_5=\sin(\pi/8)/\sin(3\pi/8)$  is the smallest positive real value of p such that (2.1) has a root on  $p_7=\sin(21/8)\pi/\sin(21/8)\pi$ . Thus,  $p_8=\pi/\sin(21/8)\pi/\sin(21/8)\pi$ .

### 4. Acknowledgments

This research is supported by the Thailand Research Fund Grant no. RTA458005 and RSA4780012. We would like to thank the referees for their valuable comments.

### References

٥

- [1] Y. Kuang, Delay Differential Equations with Applications in Population Dynamics, Mathematics in Science and Engineering, vol. 191, Academic Press, Massachusetts, 1993.
- [2] S. A. Kuruklis, The asymptotic stability of  $x_{n+1} ax_n + bx_{n-k} = 0$ , J. Math. Anal. Appl. 188 (1994), no. 3, 719–731.
- [3] S. A. Levin and R. M. May, A note on difference-delay equations, Theoret. Population Biology 9 (1976), no. 2, 178-187.
- [4] R. Ogita, H. Matsunaga, and T. Hara, Asymptotic stability condition for a class of linear delay difference equations of higher order, J. Math. Anal. Appl. 248 (2000), no. 1, 83–96.
- [5] V. G. Papanicolaou, On the asymptotic stability of a class of linear difference equations, Math. Mag. 69 (1996), no. 1, 34-43.
- [6] G. Stépán, Retarded Dynamical Systems: Stability and Characteristic Functions, Pitman Research Notes in Mathematics Series, vol. 210, Longman Scientific & Technical, Harlow, 1989.

T. Kaewong: Department of Mathematics, Faculty of Science, Chiang Mai University, Chiang Mai 50200, Thailand

E-mail address: theeradach@tsu.ac.th

Y. Lenbury: Department of Mathematics, Faculty of Science, Mahidol University, 272 Rama 6 Road, Bangkok 10400, Thailand

E-mail address: scylb@mahidol.ac.th

P. Niamsup: Department of Mathematics, Faculty of Science, Chiang Mai University, Chiang Mai 50200, Thailand

E-mail address: scipnmsp@chiangmai.ac.th

### ARTICLE IN PRESS



Available online at www.sciencedirect.com

APPLIED

MATHEMATICS

AND

COMPUTATION

ELSEVIER Applied Mathematics and Computation xxx (2005) xxx-xxx

www.elsevier.com/locate/amc

### Controllability and stability of the perturbed Chen chaotic dynamical system

Tidarut Plienpanich <sup>a</sup>, Piyapong Niamsup <sup>a,\*</sup>, Yongwimon Lenbury <sup>b</sup>

<sup>a</sup> Department of Mathematics, Faculty of Science, Chiang Mai University, Chiang Mai 50200, Thailand

### Abstract

In this paper, we study perturbed Chen chaotic dynamical system. Firstly, we study the sufficient conditions of parameters which guarantee that the equilibrium points of perturbed Chen chaotic dynamical system are asymptotically stable. Secondly, we study methods for controlling chaos such as feedback control and bounded feedback control that suppress the chaotic behavior to unstable equilibrium points. Finally, we present chaos synchronization of perturbed Chen chaotic dynamical system by using active control and adaptive control.

© 2005 Elsevier Inc. All rights reserved.

Keywords: Perturbed Chen chaotic dynamical system; Controlling chaos; Synchronization

0096-3003/\$ - see front matter © 2005 Elsevier Inc. All rights reserved. doi:10.1016/j.amc.2005.01.099

<sup>&</sup>lt;sup>b</sup> Department of Mathematics, Faculty of Science, Mahidol University, Bangkok 10400, Thailand

<sup>\*</sup> Corresponding author.

E-mail addresses: noynoy!111@hotmail.com (T. Plienpanich), piyapongniamsup@hotmail.com, seipnmsp@chiangmai.ac.th (P. Niamsup), scylb@mahidol.ac.th (Y. Lenbury).

### ARTICLE IN PRESS

T. Plienpanich et al. | Appl. Math. Comput. xxx (2005) xxx-xxx

#### 1. Introduction

In the recent years, controlling chaos and synchronization of the dynamical systems have attracted many researchers. Controlling chaos and chaos synchronization have focused on the nonlinear systems such as Chen chaotic dynamical system. Various control algorithms have been proposed to control chaotic systems. The existing control algorithms can be classified mainly into two categories: feedback and nonfeedback. In this paper, we only focus on feedback control. Linear feedback control and bounded feedback control are proposed to control chaos of the system to the equilibrium points.

In [4], Yassen's studied the optimal control of Chen chaotic dynamical system presented by

$$\dot{x} = a(y - x),$$

$$\dot{y} = (c - a)x - xz + cy,$$

$$\dot{z} = xy - bz$$

where x, y, z are state variables and a, b, c are real positive constants.

In [1], Agiza's studied the different methods to control chaotic behavior of the coupled dynamos system, where the mathematical model equations for this system are

$$\dot{x} = \mu x + y(z + \alpha),$$
  

$$\dot{y} = \mu y + x(z - \alpha),$$
  

$$\dot{z} = 1 - xy,$$

where x, y, z are state variables and  $\mu$ ,  $\alpha$  are positive constants.

In [2], Agiza and Yassen's studied synchronization of Rossler and Chen chaotic dynamical systems using active control.

In [3], Wang, Guan and Wen's paper studied adaptive synchronization for Chen chaotic system with fully unknown parameters.

The objectives of this paper are as follows. Firstly, to give sufficient conditions of parameters that make equilibrium points of perturbed Chen chaotic dynamical system to be asymptotically stable. Secondly, to apply linear feedback control and bounded feedback control for controlling chaos of the perturbed Chen chaotic dynamical system, described by

$$\dot{x} = a(y - x), 
\dot{y} = (c - a)x - xz + cy, 
\dot{z} = xy - bz + dx^2,$$
(1.1)

where x, y, z are the state variables and a, b, c, d are positive real constants.

3

### 2. Stability of the perturbed Chen chaotic dynamical system

We will study the perturbed Chen chaotic dynamical system that is described by system of ordinary differential equations (1.1).

The equilibrium points of the system (1.1) are

$$E_1 = (0, 0, 0), \quad E_2 = (\beta, \beta, \gamma), \quad E_3 = (-\beta, -\beta, \gamma),$$

where 
$$\beta = \sqrt{\frac{b\gamma}{1+d}}$$
 and  $\gamma = 2c - a$ .

**Proposition 2.1.** The equilibrium point  $E_1 = (0,0,0)$  is

- (i) asymptotically stable if a > 2c and  $ac < b^2 < 2ac$ .
- (ii) unstable if 2c > a.

**Proof.** The Jacobian matrix of the system (1.1) at the equilibrium point  $E_1 = (0,0,0)$  is given by

$$J_1 = \begin{bmatrix} -a & a & 0 \\ c - a & c & 0 \\ 0 & 0 & -b \end{bmatrix}.$$

The characteristic equation of the Jacobian  $J_1$  has the form

$$\lambda^3 + a_1\lambda^2 + a_2\lambda + a_3 = 0,$$

where

$$a_1 = a + b - c,$$

$$a_2 = b(a-c) + a(a-2c),$$

$$a_3 = ab(a - 2c),$$

$$a_1a_2 - a_3 = (ab + a^2)(a - 2c) + a(b^2 - ac) + c(2ac - b^2) + bc^2$$
.

We see that  $a_1$  and  $a_1a_2 - a_3$  satisfy the Routh-Hurwitz criteria when a > 2c and  $ac < b^2 < 2ac$ , thus the equilibrium point  $E_1 = (0,0,0)$  is asymptotically stable.  $\square$ 

**Proposition 2.2.** The equilibrium point  $E_2 = (\beta, \beta, \gamma)$  is

- (i) asymptotically stable if  $\frac{3}{2}c < a < 2c$ , b > 6c and  $\frac{1}{3} < d < 1$ .
- (ii) unstable if b < c < a and  $a < \frac{4}{3}c$ .

**Proposition 2.3.** The equilibrium point  $E_3 = (-\beta, -\beta, \gamma)$  is

- (i) asymptotically stable if  $\frac{3}{2}c < a < 2c$ , b > 6c and  $\frac{1}{3} < d < 1$ .
- (ii) unstable if b < c < a and  $a < \frac{4}{3}c$ .

### 3. Controlling chaos

In this section, the chaos of system (1.1) is controlled to one of three equilibrium points of the system. Feedback and bounded feedback control are applied to achieve this goal. We shall study in the case when equilibrium points of (1.1) are unstable. For this purpose, we assume that b < c < a and  $a < \frac{4}{3}c$ .

### 3.1. Feedback control

The goal of linear feedback control is to control the chaotic behavior of the system (1.1) to one of three unstable equilibrium points  $(E_1, E_2 \text{ or } E_3)$ . We assume that the controlled system is given by

$$\dot{x} = a(y - x) + u_1,$$
  
 $\dot{y} = (c - a)x - xz + cy + u_2,$   
 $\dot{z} = xy - bz + dx^2 + u_3,$ 

where  $u_1$ ,  $u_2$  and  $u_3$  are controllers that satisfy the following control law

$$\dot{x} = a(y - x) - k_{11}(x - \bar{x}), 
\dot{y} = (c - a)x - xz + cy - k_{22}(y - \bar{y}), 
\dot{z} = xy - bz + dx^2 - k_{33}(z - \bar{z}),$$
(3.1)

where  $E = (\bar{x}, \bar{y}, \bar{z})$  is an equilibrium point of (1.1).

3.1.1. Stability of the equilibrium point  $E_I = (0,0,0)$ 

In this case  $E = E_1$  and the controlled system (3.1) is in the form of

$$\dot{x} = a(y - x) - k_{11}x, 
\dot{y} = (c - a)x - xz + cy - k_{22}y, 
\dot{z} = xy - bz + dx^2 - k_{33}z.$$
(3.2)